A large, faint, light blue circular logo is centered in the background of the title area. It appears to be the logo of the Associação Brasileira de Ciências Mecânicas (ABCM), featuring a stylized gear or mechanical element within a circle.

REVISTA BRASILEIRA DE CIÊNCIAS MECÂNICAS

PUBLICAÇÃO DA ABCM
ASSOCIAÇÃO BRASILEIRA DE CIÊNCIAS MECÂNICAS

A Revista Brasileira de Ciências Mecânicas é uma publicação técnico-científica, da Associação Brasileira de Ciências Mecânicas. Destina-se a divulgar trabalhos significativos de pesquisa científica e/ou tecnológica nas áreas de Engenharia Civil, Mecânica, Metalúrgica, Naval, Nuclear e Química e também em Física e Matemática Aplicada. Pequenas comunicações que apresentem resultados interessantes obtidos de teorias e técnicas bem conhecidas serão publicadas sob o título de Notas Técnicas.

Os trabalhos submetidos devem ser inéditos, isto é, não devem ter sido publicados anteriormente em periódicos de circulação nacional ou internacional. Excetua-se em alguns casos publicações em anais e congressos. A apreciação do trabalho levará em conta a originalidade, a contribuição à ciência e/ou tecnologia, a clareza de exposição, a propriedade do tema e a apresentação. A aceitação final é da responsabilidade dos Editores e do Conselho Editorial.

Os artigos devem ser escritos em português, ou espanhol ou em inglês, datilografados, acompanhados dos desenhos em papel vegetal, em tamanho reduzido que permita ainda a redução para as dimensões da Revista e enviados para o Editor Executivo no endereço abaixo.

Departamento de Engenharia Mecânica — PUC/RJ
Rua Marquês de São Vicente, 225 — Gávea
22453 — Rio de Janeiro — RJ — Brasil

A composição datilográfica será processada pela própria secretaria da RBCM de acordo com as normas existentes.

The Revista Brasileira de Ciências Mecânicas (Brazilian Journal of Mechanical Sciences) is a technical-scientific publication, sponsored by the Brazilian Association of Mechanical Sciences. It is intended as a vehicle for the publication of Civil, Mechanical, Metallurgical, Naval, Nuclear and Chemical Engineering as well as in the areas of Physics and Applied Mathematics. Short communications presenting interesting results obtained from well-known theories and techniques will be published under heading of the Technical Notes.

Manuscripts for submission must contain unpublished material, i.e., material that has not yet been published in any national or international journal. Exception can be made in some cases of papers published in annals or proceedings of conferences. The decision on acceptance of papers will take into consideration their originality, contribution to science and/or technology, writing clearness, propriety of the subject and presentation. The Editors and the Editorial Committee are responsible for the final approval.

The papers must be written in Portuguese, Spanish or English, typed and with graphics done on transparent white drawing paper in reduced size in such a way as to permit further reduction to the dimensions of the Journal, and sent to the Executive Editor at the following address.

PUC — Pontifícia Universidade Católica do RJ
Departamento de Engenharia Mecânica
Rua Marquês de São Vicente, 225 — Gávea
22453 — Rio de Janeiro, RJ — Brasil

The final typing will be done by the secretary of RBCM according to the journal norms.



EDITOR
RESPONSÁVEL

Rubens Sampaio

EDITOR
EXECUTIVO

J. M. Freire

CONSELHO
EDITORIAL

Abimael F. D. Loula
Arthur J. V. Porto
Berend Snoeijer
Bernardo Horowitz
C. S. Barcellos
D. E. Zampieri
Duraíd Mahrus
E.O. Taroco Aliano
F. Venâncio Filho
F. E. Mourão Saboya
Giulio Massarani
Guillermo Creuss
Hans Ingo Weber
Henner A. Gomide
Jan Leon Scieszko
Jerzy T. Sielawa
J. J. Espíndola
Liu Hsu
Maurício N. Frota
Miguel H. Hirata
Nelson Back
Néstor Zouain
Nivaldo L. Cupini
O. Maizza Neto
Pedro Carajilescov
Sergio Colle

Conselho da ABCM - Biênio 86/87

167

Machine-foundation-soil Interaction; combined
continuum and boundary element approach

169

L. Gaul

Institut für Mechanik

University of the German Armed Forces Hamburg

Toward the utilization of computer intelligence in
metal machining

199

Dr. Hejat Olgac

University of Connecticut - USA

Sobre a interpretação do tensor parcial de tensão e da
força difusiva em misturas sólido-fluido

219

Rogério Martins Saldanha da Gama - Membro da ABCM

LNCC/CNPq

Rubens Sampaio - Membro da ABCM

DEM-PUC/RJ

Stability analysis of dissipative nonlinear dynamical al
systems

232

Edwin J. Kreuzer

Institute B of Mechanics

University of Stuttgart

Pfaffenwaldring 9

D-7000 Stuttgart 80, F. R. G.



**A REVISTA BRASILEIRA DE CIÊNCIAS MECÂNICAS
É PUBLICADA COM O APOIO**

**DO CNPq E FINEP
COMPANHIA VALE DO RIO DOCE
IBM DO BRASIL**

Conselho da ABCM eleito para o Biênio 86/87

Eng^o Carlos Alberto Couto, FINEP
Dr. Edgardo Taroco, LNCC/CNPq
Dr. Hazim Ali Al-Qureshi, ITA
Dr. Henner Alberto Gomide, UFU
Suplente - Dr. Jaime Tupiassú Pinto de Castro, PUC/RJ
Eng^o José Augusto R. do Amaral, NUCLEN
Suplente - Eng^o José Carlos Balthazar, UnB
Prof. José de Mendonça Freire, PUC/RJ
Suplente - Dr. Kazuo Hatakeyama, CEPED/BA
Dr. Raúl A. Feijóo, LNCC/CNPq
Dr. Rubens Sampaio Filho, PUC/RJ
Dr. Tito Luiz da Silveira, Fund. Souza Marques
Dr. Valder Steffen Junior, UFU

MACHINE-FOUNDATION-SOIL INTERACTION; COMBINED CONTINUUM AND BOUNDARY ELEMENT APPROACH

L. Gaul

Institut für Mechanik

University of the German Armed Forces Hamburg

ABSTRACT

A theoretical approach is developed and programmed to analyze the three-dimensional dynamic response of machines on foundations interacting with soil. Structures and soil are coupled by means of a substructure technique. The substructure behavior of soil is treated for rigid and flexible foundation slabs of arbitrary shape. Surface foundations as well as embedded foundation can be taken into account. The viscoelastic field equations of soil halfspace are solved by a continuum approach. Semianalytical solutions are superimposed by Fourier's integral theorem. The excavated soil for embedded foundation slabs is described by substructure deletion by means of combining the continuum approach for the halfspace with the boundary element approach for the excavated soil domain. The difficulties of pure finite element and boundary element discretizations, namely introduction of artificial soil boundaries and truncation of discretization respectively, are circumvented by the present method. The interaction between a single turbomachinery frame foundation and soil as well as the interaction through the underlying soil between adjacent block foundations are considered. The assumptions of perfectly smooth and perfectly welded contact at the interface between soil and bases bound the influence of shear stresses. The impact of foundation flexibility with respect to rotor vibrations is discussed. Experimental studies describe the measured sine sweep response and vibration modes of a small scale frame foundation and a rigid circular block foundation on compressed sand.

INTRODUCTION

The prediction of machine vibrations by theoretical approaches as well as the modification of response after construction often require taking the interaction between machine, foundation-structure and subsoil into account. Three examples are given. Figure 1 shows a discretized model of a drilling machine with long foundation slab on soil. The impact of static soil-structure interaction was calculated and measured by Thurat (1978). A base for the dynamic analysis is given by the soil model in the present paper.

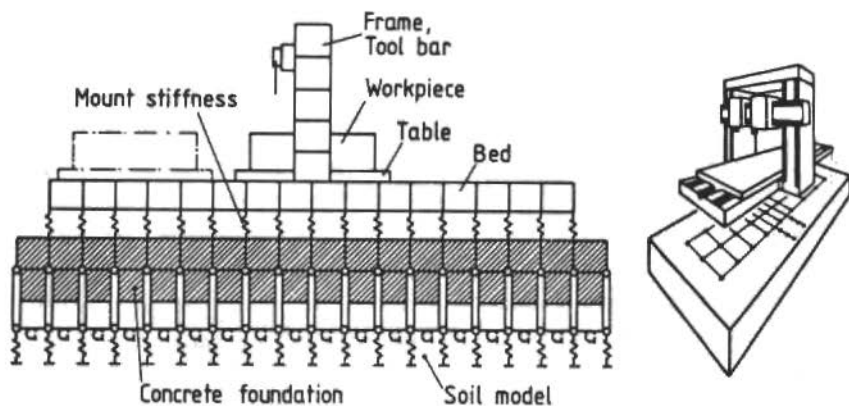


Figure 1. Model of drilling machine, foundation slab and soil

A multi body of a forging hammer (Fig. 2) is coupled with a viscoelastic truncated cone model of soil (Knobloch and Gaul 1975). Thurat (1978) calculated and measured the transient response. Novak (1982) treats a hammer foundation as a system of two masses on a viscoelastic halfspace including embedment effects.

The global response of turbomachinery frame foundation e.g. the low-tuned steel foundation with concret raft (Dietz 1972) of Figure 3 or the response of block foundations are calculated and studied experimentally by small scale models in the present paper. Dynamic response results from active excitations by rotor unbalances, short circuit moments and shaft misalignments or by passive seismic excitation.

The function of the foundation is not only to support the weight of the expensive equipment; the light upper steel plate on flexible columns (Figure 3) minimizes the amplitudes of shaft whirling relative to the bearings. Although the tendency often prevails to treat the rotor, the frame and the foundation as if they were independent, actually all these substructure interact. This interaction was treated by Gasch and Sarfeld (1980) for a Laval shaft on a block foundation and by Aboul-Ella and Novak (1978) for a turbogenerator on a pile-supported frame foundation. The horizontal soil stiffness in the first paper was calculated by Gaul (1979), the vertical soil stiffness matrix of the second paper by Gaul (1977).

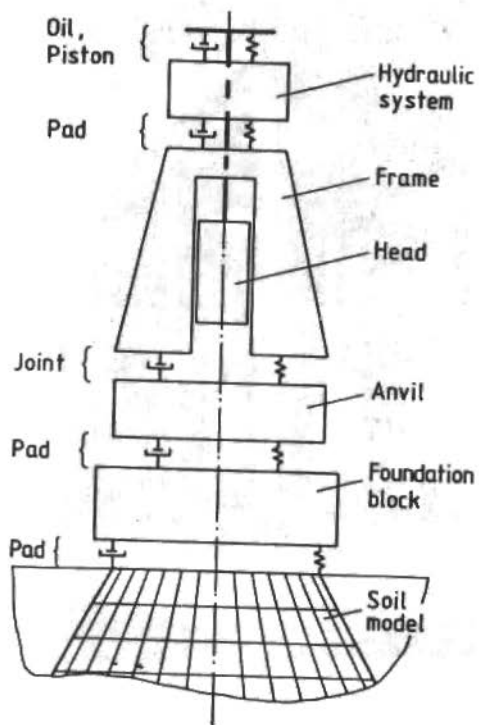


Figure 2. Model of hammer, foundation and soil

Methods for simulation of soil-structure interaction often take advantage of substructure techniques by coupling the model of structure and base plate with the model of the substructure soil. Structures are usually discretized by finite elements or can be treated in special cases by analytical dynamic stiffness matrices as in the present paper. Besides simplified soil models (Gaul and Plenge 1983) the substructure soil is usually described by finite elements (Waas 1972), halfspace theory (Holzlöhner 1969, Gaul 1980) or boundary elements (Ottensreuer 1982).

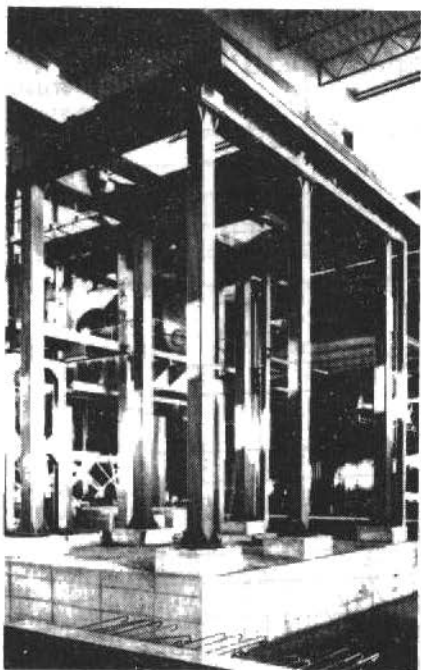


Figure 3. Low-tuned steel foundation with concrete raft

Finite elements do also allow for a simultaneous discretization of structure and soil. The method is equally applicable to embedded foundations and inhomogeneous soil. It has however serious disadvantages when applied to three-dimensional problems since it requires extensive, complicated and expensive data management. Energy radiation travelling out to infinity by waves (geometrical damping) can be represented approximately by semi-infinite elements, which do only simulate the infinite extension in the horizontal direction (Waas 1972).

The halfspace theory presented here treats the substructure soil separately. The soil is assumed to be an elastic (Holzlöhner 1969) or viscoelastic (Gaul 1980) homogeneous halfspace. Dynamic stiffness matrices of the discretized soil surface can be coupled with rigid or flexible base plates or arbitrary shape (Sarfeld and Fröhlich 1980, Gaul 1980). Three-dimensional motion of structures can be described even in the high frequency range. Soil inhomogeneity has to be approximated by one or two layers or the concept of equivalent moduli. Embedment has to be approximated as well.

As another tool the boundary element method proved to be well suited to handle soil dynamics problems. It is possible to calculate embedded structures (Dominguez 1978, Huh, Schmid and Ottenstreuer 1983) as well as layered media.

Viscoelastic material properties and coupling effects of neighbouring foundations can be described by all three methods.

COUPLING OF SUBSTRUCTURES

The neighbouring structures (Fig. 4) interact with soil. The transfer behaviour of the three substructures can be described, in the frequency domain of Fourier transform by dynamic stiffness matrices $[K(i\omega)]$ including inertia, damping and stiffness properties.

The substructure matrices of soil $[K]$ and both structures $[K]_I$, $[K]_{II}$ are coupled by compatibility requirements of generalized displacements $\{U_c\}$ and forces $\{F_c\}$ at the contact nodes of the interfaces I and II. Seismic excitation requires the input of generalized displacements $\{U_c\}$ at the unloaded interfaces generated by incoming waves. With the generalized forces of active excitation $\{P\}$ the substructure equations are give by

$$\begin{aligned}
 \text{I} \\
 [K(i\omega)] \begin{bmatrix} \{U\} \\ \{U_C\} \end{bmatrix} &= \begin{bmatrix} \{P\} \\ -\{F_C\} \end{bmatrix} \\
 \text{II} \\
 [K(i\omega)] \begin{bmatrix} \{U_C\} \\ \{U\} \end{bmatrix} &= \begin{bmatrix} -\{F_C\} \\ \{P\} \end{bmatrix}
 \end{aligned} \tag{1}$$

and

$$\text{S} \\
 [K(i\omega)] \begin{bmatrix} \{U_C\} - \{V_C\} \\ \{U_C\} - \{V_C\} \end{bmatrix} = \begin{bmatrix} \{F_C\} \\ \{F_C\} \end{bmatrix} \tag{2}$$

where the generalized displacements of structures $\{U\}$ are separated from those at the interfaces $\{U_C\}$. With given excitation data Eqs. (1) and (2) lead to the generalized displacement response of the coupled system by solving

$$\begin{bmatrix} \text{I} \\ [K] \text{S} \\ \text{II} \\ [K] \end{bmatrix} \begin{bmatrix} \{U\} \\ \{U_C\} \\ \{U\} \\ \{U_C\} \end{bmatrix} = \begin{bmatrix} \{P\} \\ \{0\} \\ \{0\} \\ \{P\} \end{bmatrix} + \begin{bmatrix} \text{S} \\ [K] \end{bmatrix} \begin{bmatrix} \{V_C\} \\ \{V_C\} \end{bmatrix} \tag{3}$$

The solution of Eq. (3) leads to complex amplitudes $\{U\} = \{U_R\} = \{U_R\} + i\{U_I\}$ corresponding to real displacements $\{u(t)\} = \{U_R\} \cos \omega t - \{U_I\} \sin \omega t$ for time harmonic excitation or to Fourier transformed displacements, corresponding to transient excitation. Calculation of transient response requires the inverse transformation which can be computed efficiently by the fast Fourier transform algorithm.

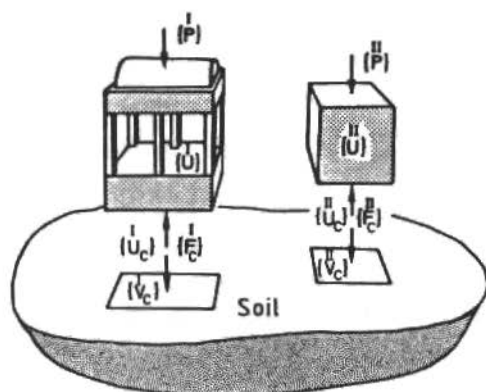


Figure 4. Substructures of soil-structure interaction

SUBSTRUCTURE SOIL

Interaction of Soil with Rigid and Flexible Base Plates

The substructure behavior of soil is calculated by the halfspace approach for idealized rigid base plates and for flexible plates. The plane interfaces of soil (Fig. 5) are loaded by forces F_i and moments M_i generated by the structures. Solutions of the field equations of soil have to fulfill mixed boundary values:

- rigid bases require plane displacement fields at the interfaces,
- the soil surface is stressfree elsewhere.

While rigorous formulations by dual integral equations (Gaul 1980a) lead to approximate solutions only for simple base geometries, the presented superposition method provides solutions for arbitrary shapes and allows for taking flexible base plates into account.

Arbitrary shapes are modelled by subdividing the interfaces into rectangular surface elements. The continuous stress distributions in the interfaces are discretized by locally constant pressures in each element, acting harmonically in time. Each loaded surface element in Fig. 5 defines a stress boundary value problem of the halfspace. The assumption of decoupled horizontal and vertical displacement fields simplifies the analysis. Only vertical displacements generated by the load components in Fig. 5 are calculated. The horizontal displacements (Gaul 1977) generated

by the missing load components are superimposed. To bound the influence of shear stresses at the vertically moving interfaces:

- smooth contact with vanishing shear stresses,
- welded contact with vanishing horizontal displacements.

are compared. Semianalytical solutions of both boundary value problems lead to flexibility influence matrices. One complex, frequency dependent matrix element \bar{h}_{ij} relates the complex displacement \bar{w}_{ij} in the middle of element i to the amplitude $(\bar{p}A)_j$ of the time harmonic force acting at element j .

Displacement superposition leads to

$$\bar{w}_i = \bar{h}_{ij} (\bar{p}A)_j \quad (4)$$

written with the flexibility matrix [h]

$$\{w\} = [h] \{F\}$$

or with the inverse dynamic stiffness matrix $\overset{S}{[K]}$ of soil halfspace

$$\{F\} = \overset{H}{[K]} \{w\} .$$

For rigid bases the corresponding interface stress distribution is determined by requiring:

- the displacement boundary conditions of the plane interface displacement fields to be fulfilled in the center of each soil element,
- the result of the interface stresses to be equivalent to the halfspace load resultants.

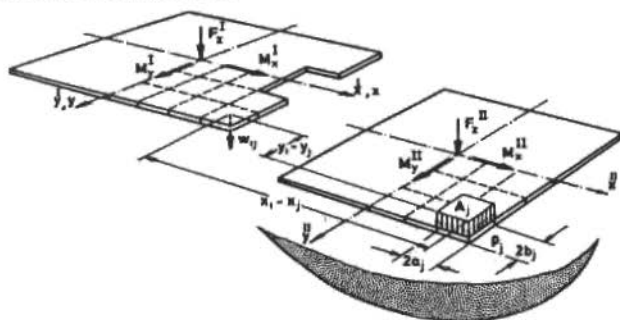


Figure 5. Mixed boundary value problem of soil. Stress boundary value problem of one interface soil element

The interaction of soil with flexible base plates requires a plate discretization by finite elements compatible to the soil element discretization (Fig. 6).

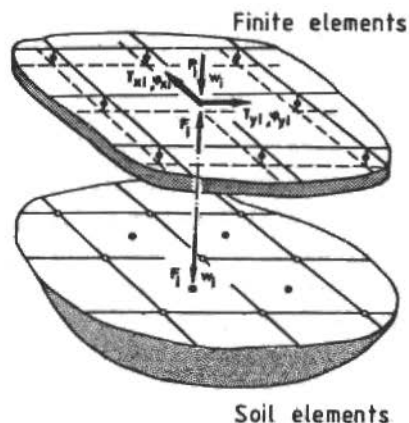


Figure 6. Base plate interacting with soil.
Coupled finite elements and soil elements

The equations of motion of the discretized base plate, which is loaded by nodal external forces $\{P\}$, moments $\{T\}$ and halfspace reactions $\{F\}$, are partitioned with respect to the translational $\{w\}$ and rotational $\{\phi\}$ degrees of freedom. Coupling of mass matrix $[M]$ and viscoelastic stiffness matrix $[K]$ of the base plate with soil is achieved by displacement compatibility at the plate nodes and soil element centers. Expressing the unknown displacements $\{w\}$ by Eq. (4) avoids the inversion of the flexibility matrix $[h]$ and leads to a linear set of complex equations

$$\left[\begin{array}{c|c} (-\omega^2 [M_V] + [K_V]) [h] + [E] & -\omega^2 [M_{V\phi}] + [K_{V\phi}] \\ \hline (-\omega^2 [M_{V\phi}]^T + [K_{V\phi}]) [h] & -\omega^2 [M_\phi] + [K_\phi] \end{array} \right] \begin{Bmatrix} \{F\} \\ \{\phi\} \end{Bmatrix} = \begin{Bmatrix} \{P\} \\ \{T\} \end{Bmatrix} \quad (5)$$

- from which the halfspace reaction $\{F\}$, determining the soil pressure distribution, and the translational and rotational degrees of freedom $\{\phi\}$ and with Eq. (4) $\{w\}$ follow. The results have to be interpreted as complex amplitudes for time harmonic excitations or as Fourier transform of transient response.

Flexibility Matrix of Soil Halfspace, Stress Boundary Value Problems for Smooth and Welded Contact

The solutions of the stress boundary value problems of halfspace, loaded vertically on one surface element (Fig. 5), are given semianalytically by the Fourier integral for smooth and welded contact. Compared with elastic halfspace theories, a better approximation of the rheological properties of soil is given here by using viscoelastic constitutive equations. It turns out, that the energy dissipation by material damping is of considerable influence when the geometrical damping by wave radiation is of same order of magnitude. The equations of motion of the viscoelastic continuum in terms displacements $u_i(x_j, t)$

$$\int_{-\infty}^t E_D(t-\tau) \frac{\partial u_{j,ji}}{\partial \tau} d\tau - e_{ijk} e_{klm} \int_{-\infty}^t G(t-\tau) \frac{\partial u_{m,lj}}{\partial \tau} d\tau = \rho \frac{\partial^2 u_i}{\partial t^2} \quad (6)$$

are decomposed by

$$u_i = \phi_{,i} + e_{ijk} \psi_{k,j} \quad (7)$$

in two wave equations for the scalar and the vector potential ϕ and ψ_k respectively

$$\int_{-\infty}^t E_D(t-\tau) \frac{\partial \phi_{,ll}}{\partial \tau} d\tau = \rho \frac{\partial^2 \phi}{\partial t^2} \quad (8)$$

$$\int_{-\infty}^t G(t-\tau) \frac{\partial \psi_{k,ll}}{\partial \tau} d\tau = \rho \frac{\partial^2 \psi_k}{\partial t^2} .$$

This representation is complete (Gaul 1980) if the constraint condition $\psi_{k,k} = 0$ is satisfied. Steady state harmonic motion

$$u_i(x_j, t) = \text{Re}\{\bar{u}_i(x_j) \exp(i\omega t)\} \quad (9)$$

leads to reduced wave equations for dilatation $\epsilon = u_{l,l} = \phi_{,ll}$ and rotations $2\omega_k = e_{kij} u_{j,i} = -\psi_{k,ll}$ with relaxation functions of plane dilatation $E_D(t)$ and shear $G(t)$ replaced by complex moduli

$$E_D^*(i\omega) = \lambda^*(i\omega) + 2G^*(i\omega) \text{ and } G^*(i\omega) \\ \bar{\epsilon}_{,ll} + \frac{\rho\omega^2}{E_D^*} \bar{\epsilon} = 0, \quad \bar{\omega}_{k,ll} + \frac{\rho\omega^2}{G^*} \bar{\omega}_k = 0. \quad (10)$$

Excluding reflections, solutions are given by

$$\bar{\epsilon} = A \exp[-\alpha_D z + i(\beta x + \gamma y)], \\ \bar{\omega}_k = B_k \exp[-\alpha_S z + i(\beta x + \gamma y)] \quad (11)$$

where $\text{Re}(\alpha_{D,S}) \geq 0$, $\bar{\omega}_{k,k} = 0$. Displacement field and stress field and stress field are superimposed by these solutions

$$\bar{u}_i = -\bar{\epsilon}_{,i} + 2e_{ijk} \bar{\omega}_{k,j} \\ \bar{\sigma}_{ij} = [E_D^*(i\omega) - 2G^*(i\omega)] \bar{u}_{k,k} \delta_{ij} + G^*(i\omega) (\bar{u}_{i,j} + \bar{u}_{j,i}) \quad (12)$$

with A, B_k determined by the boundary conditions. The stress boundary value problem is solved by superposition of harmonic vertical displacement waves at the halfspace surface $z = 0$

$$w(x, y, 0, t) = \\ = \bar{H}^{\beta, \gamma, \omega}(\beta, \gamma, \omega) \bar{p}(\beta, \gamma) \exp[i(\beta x + \gamma y + \omega t)] \quad (13)$$

generated by the stress wave

$$-\sigma_{zz}(x, y, 0, t) = p(x, y, t) = \\ = \bar{p}(\beta, \gamma) \exp[i(\beta x + \gamma y + \omega t)] \quad (14)$$

propagating with phase velocity $v = \omega/\zeta$, where $\zeta = (\beta^2 + \gamma^2)^{1/2}$. Real and imaginary part of the complex wave compliances \bar{H}^S, \bar{H}^W corresponding to smooth (s) and welded (w) contact are plotted in Fig. 7 versus the velocity ratio v/v_s .

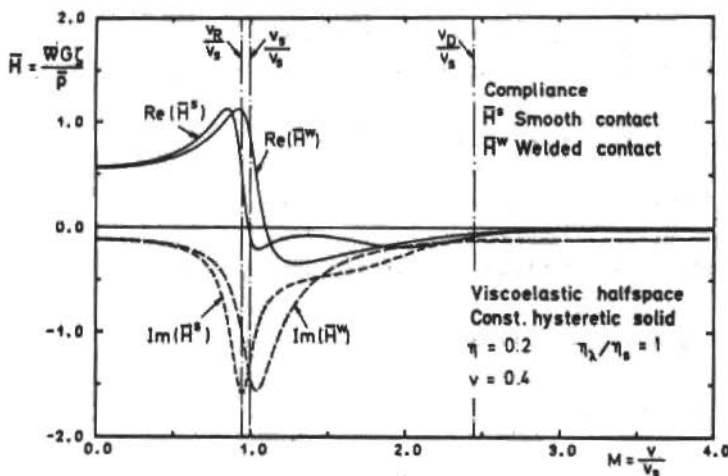


Figure 7. Wave compliances of viscoelastic halfspace

The compliance show the features of a single-degree-of-freedom system. Welded contact leads to a resonant condition at the shear wave velocity $v_s = \sqrt{G/\rho}$, smooth contact leads to resonance associated with the slightly slower Rayleigh wave speed v_R . Fig. 8 shows an experimental setup (Crandall et al. 1971) by which the damping factors $\eta_D(\omega)$, $\eta_S(\omega)$ of the complex moduli $E_D^* = E_D(1 + i\eta_D)$, $G^* = G(1 + i\eta_S)$ and Poisson's ratio can be measured. The damping factors are related by

$$\eta_D = \eta_\lambda + (\eta_S - \eta_\lambda) (1 - 2\nu)/(1 - \nu),$$

with damping factor η_λ of Lamé modulus $\lambda^* = \lambda(1 + i\eta_\lambda)$.

Taking advantage of available measured data, results are presented for the constant hysteretic solid and Kelvin-Voigt-solid leading to damping factors

$$\eta_{S,\lambda}(\omega) = \eta_{S,\lambda} \quad \text{and} \quad \eta_{S,\lambda}(\omega) = a_0 \xi_{S,\lambda}$$

respectively, where $a_0 = \omega a / v_s$ is a frequency parameter with characteristic length a .

The obtained harmonic solutions are now superimposed by integrating with respect to the wave numbers β, γ in Fourier's integral theorem

$$w(x, y, z, t) = \frac{1}{2\pi} \iint_{-\infty}^{\infty} \bar{H}^{S, W}(\beta, \gamma, \omega) \bar{p}(\beta, \gamma) \times \\ \times \exp[i(\beta x + \gamma y + \omega t)] d\beta d\gamma \quad (15)$$

with

$$\bar{p}(\beta, \gamma) = \frac{2p_j}{\pi} \left(\frac{\sin \beta a_j \sin \gamma b_j}{\beta \gamma} \right)$$

being the two-dimensional Fourier transform of the exciting stress field (Fig. 5) at one surface element of area $4a_j b_j$. The elastic halfspace leads to improper integrals due to poles the compliance in Eq. (15) at the shear wave and the Rayleigh wave speed. Solutions can be obtained by choosing Cauchy's principal value and performing a contour integration in the complex plane. Here a different technique is used. Because the viscoelastic halfspace yields finite resonance amplifications instead of poles (Fig. 7), the integral of Eq. (15) is no longer improper with respect to the integrand and can be integrated directly.



Figure 8. Clay sandwich for alternating dilatation and shear tests

By pointwise evaluation of the complex surface displacement field, the soil flexibility matrix [h] of Eq. (4) is obtained with elements

$$h_{ij} = \bar{w}(x_i, y_i) / [\bar{p}A(x_j, y_j)].$$

Flexibility Matrix of Excavated Soil Halfspace for Coupling With Embedded Base Plates by Substructure Deletion

The dynamic stiffness matrix of substructure soil calculated analytically by solving the field equations of the halfspace can be applied not only for describing surface foundations but also for embedded foundations. The effect of embedment can be taken into account by substructure deletion utilizing the available continuum and discrete solution techniques.

Finite element discretizations of soil require to introduce artificial boundaries at some distance from the base plate although the foundation medium is geometrically unbounded. When applying the boundary element method, surface discretization too has to be truncated at some distance from the base implying a discretization error.

These difficulties are circumvented in the present approach by employing the substructure deletion technique (Fig. 9).

The dynamic stiffness matrix of the excavated halfspace $[K_e^H]$ is calculated from the known dynamic stiffness matrix of the halfspace obtained by the continuum approach $[K^H]$ and the dynamic stiffness matrix $[K^E]$ of the excavated domain.

Finite element discretization of the excavated domain (Dasgupta 1980) requires to condense the internal nodal degrees of freedom out and leads to $[K^E] = [K] - \omega^2 [M]$ by static condensation.

The author applies surface discretization by the boundary element method, where condensation drops out.

The boundary nodes are divided in those at the ground level surface $\{u_s^E\}$ and those at the excavation surface $\{u_e^E\}$. Interface conditions at the ground level surface require identity of nodal forces and displacements at the halfspace surface and excavated domain surface:

$$\{F_s^H\} = \{F_s^E\}, \quad \{u_s^H\} = \{u_s^E\}$$

At the excavated surface equilibrium of nodal forces $\{F_e^E\} + \{F_e^H\} = \{0\}$ and displacement compatibility $\{U_e^E\} = \{U_e^H\}$ has to be fulfilled.

As simultaneous prescription of nodal forces and displacements on the common boundary points is required, Dasgupta (1979) demonstrated that well posedness can be guaranteed if and only if the discrete models can reproduce those results which are the counterparts of Almansi's triviality theorem (Almansi 1907).

These requirements and the known dynamic stiffness matrices of halfspace and excavated domain lead to the dynamic stiffness matrix of the excavated $[K_e^H]$ (fig. 9). Interaction with an embedded base plate can be calculated by coupling the dynamic stiffness matrices.

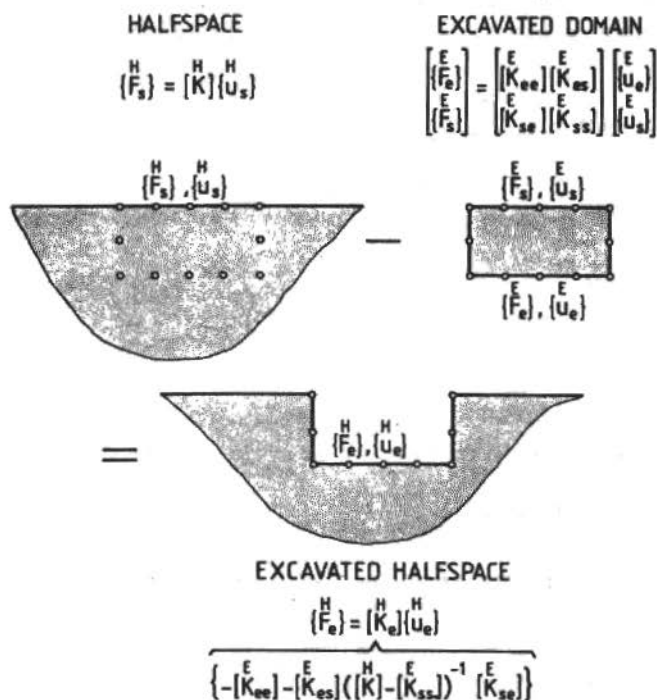


Figure 9. Flexibility of excavated soil halfspace by substructure deletion

SUBSTRUCTURE FRAME FOUNDATION AND SHAFT

As an example of a sensitive structure interacting with soil a frame foundation (Fig. 3) is considered. Only the global vibration behaviour in the low frequency range is treated on the bases of a simplified model (Fig. 9) which is suited for comparisons with experimental results from small scale frame foundations.

The rigid upper plate is excited harmonically by the force F_i and torque T_i^D generated e.g. by the unbalances of a Laval rotor with excentricity e . Upper plate and base plate are connected by flexible columns, rigid bearings and rotating disk are connected by the flexible shaft. The halfspace reactions are reduced to point B in the interface. The three-dimensional motion of upper plate, base plate and disk are described by displacement coordinates v_i, u_i, w_i and the angles of small rotations ϕ_i, ψ_i, α_i respectively. The geometrically linearized Newton-Euler equations of motion yield with simbols, coordinates and constraints from Fig.10.

- for the upper plate with mass M , inertia tensor I_{ij}^D

$$\begin{aligned}
 & I_{ij}^D \ddot{\phi}_j + M e_{ijk} r_j^c \ddot{v}_k = \\
 & = - \sum_{\alpha=1}^{\beta} (e_{ijk} r_j^{\alpha} P_k^F + M_i^{\alpha} F) + T_i^D \\
 & M(\ddot{v}_i - e_{ijk} r_j^c \ddot{\phi}_k) = \\
 & = - \sum_{\alpha=1}^{\beta} P_i^{\alpha} F + K_i^D
 \end{aligned} \tag{16}$$

- for the base plate with mass m , inertia tensor J_{ij}^A

$$\begin{aligned}
 & J_{ij}^A \ddot{\phi}_j + m e_{ijk} x_j^c \ddot{u}_k = \\
 & = - \sum_{\alpha=1}^{\beta} (e_{ijk} x_j^{\alpha} P_k^S + M_i^{\alpha} S) - (M_i^B + e_{ijk} x_j^0 F_k^B) \\
 & m(u_i - e_{ijk} x_j^c \ddot{\phi}_k) = - \sum_{\alpha=1}^{\beta} P_i^{\alpha} S - F_i^B.
 \end{aligned} \tag{17}$$

- for the rotating disk with mass m_d , inertia tensor θ_{ij}^d , angular velocity ω

$$\theta_{ij}^d \ddot{\alpha}_j + \theta_{11}^d \omega (\delta_{11} \dot{\alpha}_1 - \delta_{13} \dot{\alpha}_3) = -T_i^d \quad (18)$$

$$m_d \ddot{w}_i = k_i^d + m_d e \omega^2 (\cos \omega t \delta_{1i} - \sin \omega t \delta_{3i})$$

Flexible columns and flexible shaft are treated as space beams with distributed mass. The effects of shear, rotary inertia, static axial force and viscoelastic material properties are considered in dynamic, complex value stiffness matrices (Aboul-Ella, Novak 1980, Gaul 1980)

- column α

$$\begin{pmatrix} M_i^F \\ P_i^F \\ M_i^S \\ P_i^S \end{pmatrix}^\alpha = [K_{i\ell}]^\alpha \begin{pmatrix} \phi_\ell \\ v_\ell - e_{\ell mn}^{\alpha} x_m^{\alpha} \phi_n \\ \phi_\ell \\ u_\ell - e_{\ell mn}^{\alpha} x_m^{\alpha} \phi_n \end{pmatrix} \quad (19)$$

- shaft

$$\begin{pmatrix} M_i^d \\ K_i^d \\ M_i^D \\ K_i^D \end{pmatrix} = [K_{i\ell}]^d \begin{pmatrix} \alpha_\ell \\ w_\ell \\ \phi_\ell \\ v_\ell \end{pmatrix} \quad (20)$$

In the frequency domain Eqs. (16) to (20) lead to a substructure equation like Eq. (1)

$$[K(i\omega)] \begin{bmatrix} \{U\} \\ \{U_c\} \end{bmatrix} = \begin{bmatrix} \{P\} \\ -\{F_c\} \end{bmatrix} \quad (21)$$

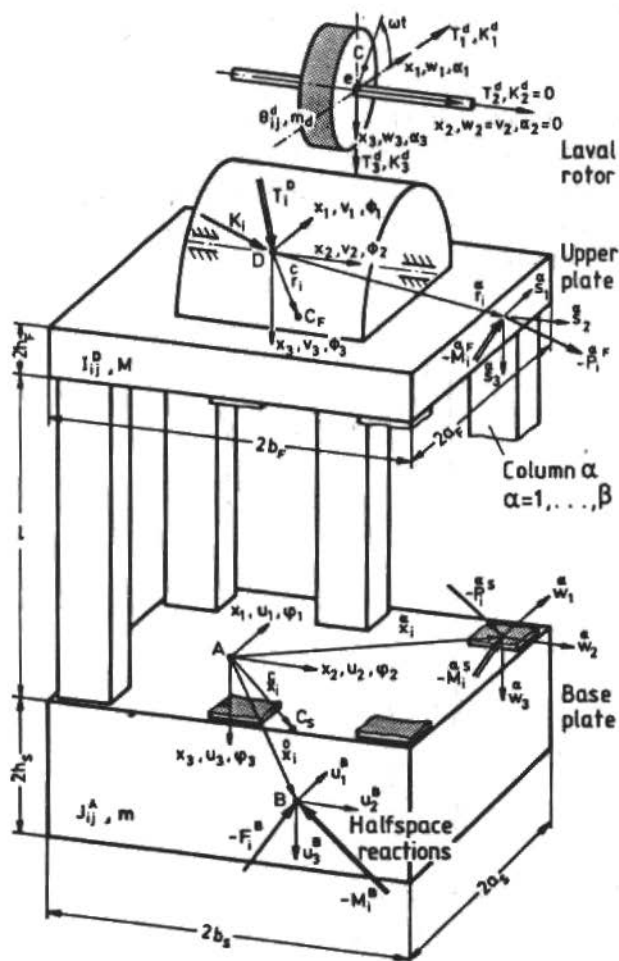


Figure 10. Rotor on frame foundation interacting with soil

CALCULATED RESULTS OF SOIL-STRUCTURE INTERACTION

Lumped Parameters of Substructure Soil

The solution of the mixed boundary value problem, describing the interaction between one rigid base and soil leads to the complex elements of the soil stiffness matrix (Eq. 2) $\bar{K}_{ij}^S = c_{ij}(a_0) + i a_0 d_{ij}(a_0)$, which can be modelled as lumped parameters of soil. The spring and damping coefficients $c_z(a_0)$ and $d_z(a_0)$ corresponding to vertical vibration of rigid square base are plotted in Fig. 10 versus the frequency parameter $a_0 = \omega a/v_s$. The spring coefficient, describing elastic restoring forces and inertia forces, is slightly higher in the low frequency range for welded contact than for smooth contact. This is due to the displacement constraint at the half-space geometrical damping primarily associated with the Rayleigh wave for smooth contact. Thus the damping coefficient d_z^S exceeds d_z^W . In the present paper all lumped parameters additionally depend on the energy dissipation of soil governed by viscoelasticity. One important result of the analysis with respect to the uncertainties of the contact boundary conditions is that it makes little difference whether the contact at the interface is smooth or welded.

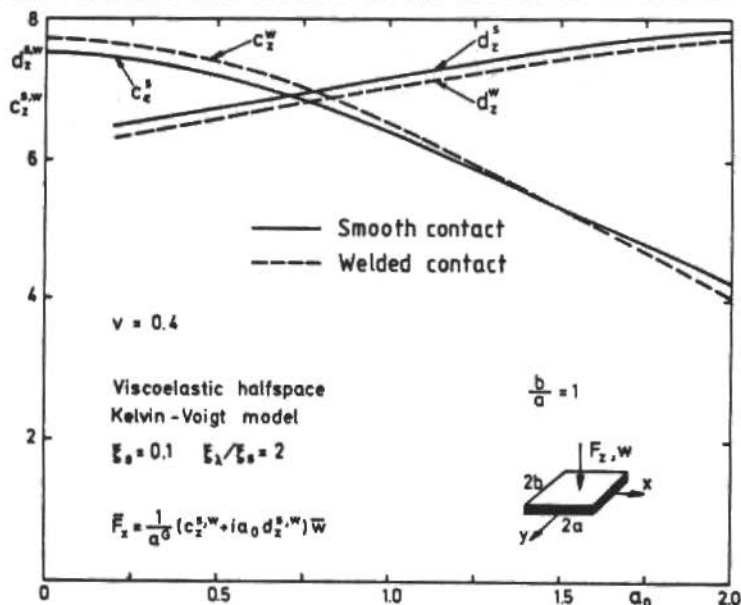


Figure 11. Spring and damping coefficient of soil for vertical motion of a rigid base

Interaction Between Two Structures

Real and imaginary parts of the complex interface pressure distribution are given in Fig. 12 corresponding to the interaction through the underlying soil between two rigid structures, which are excited by forces P_Z^I, P_Z^{II} and torques T_X^I, T_Y^{II} due to rotating unbalanced masses, acting with a phase shift.

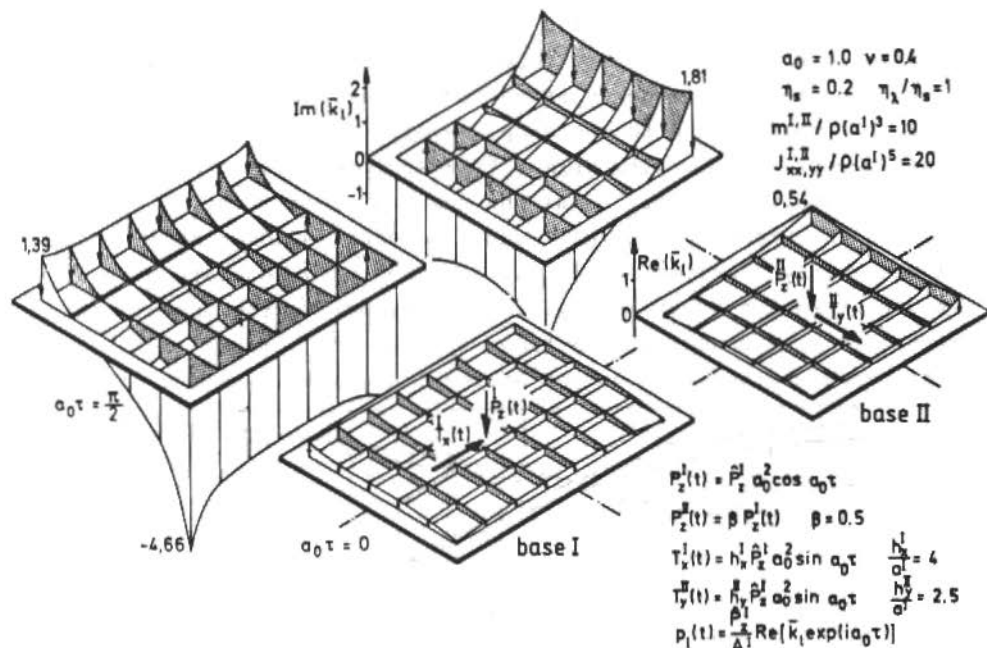


Figure 12. Interface pressure distribution for adjacent excited bases

Dynamic Response of Machine Foundations

The dynamic response of a frame foundation (Fig. 13) with eight concrete columns is evaluated as an application of the presented substructure technique. The system is excited by an unbalanced rigid rotor. The magnification functions in Fig. 12 describe the amplitudes of horizontal displacements v_1, u_1 and vertical displacements v_3, u_3 . According to Fig. 9 v_1 belongs to the upper plate and u_1 to the base plate. The coupled rocking and

horizontal motion gives rise to two resonant amplifications indicated by the horizontal displacement amplitudes within the regarded frequency range. The resonant amplifications are affected by material damping of soil because rocking motion cause only small geometrical damping by wave radiation (Gaul, 1980). This indicates vertical motion being associated with strong geometrical damping. Frequency independent static lumped parameters of soil lead to the compared deviations of response. The vibration modes in Fig. 14 show the coupling between a rocking and sliding motion.

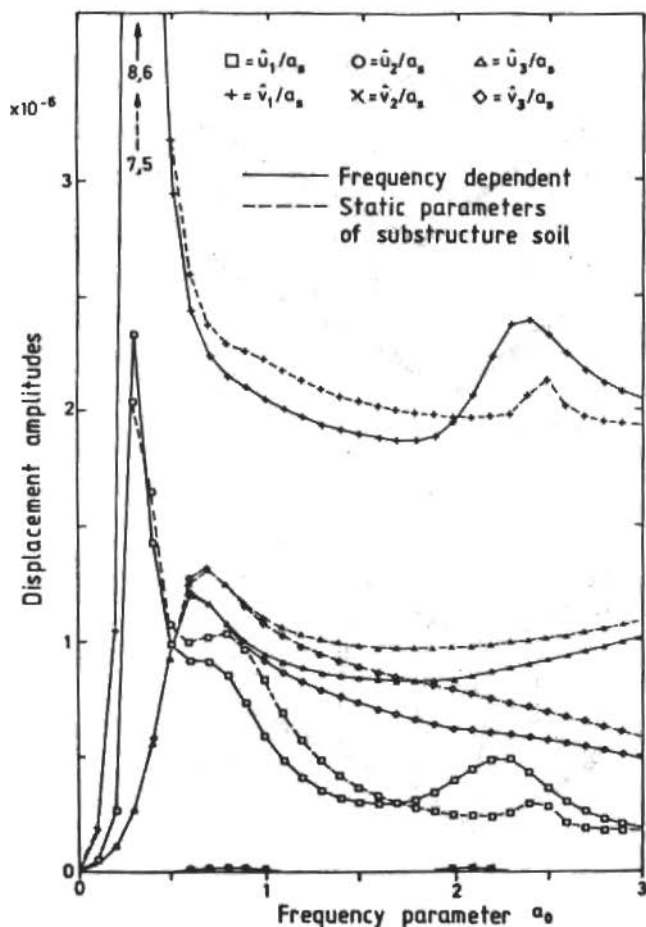


Figure 13. Response of frame foundation on soil

Rigid columns of the frame foundation simplify Eqs. (16) to (21) and lead to the description of a Laval rotor on a block-foundation (Gasch and Sarfeld 1980, Krämer 1984). If only a planar motion is considered, the system has 5 degrees of freedom. Fig. 5 compares the response of the rotor on a rigid foundation with the response corresponding to a flexible foundation.

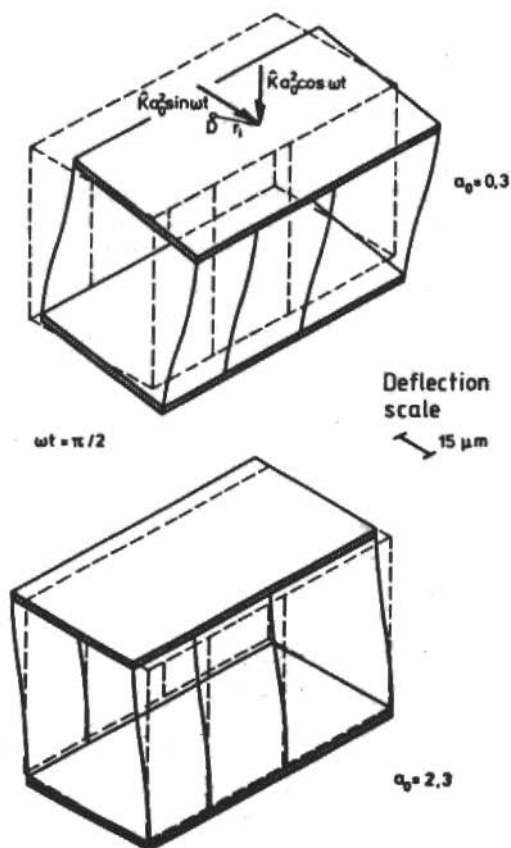


Figure 14. Vibration modes of frame foundation on soil

Analogous to the frame foundation (Fig. 13) the first three resonant amplifications are predominately due to the foundation, while the last two are governed by the rotor. The foundation influence splits one resonant frequency of the rotor in two of the combined structure with lower amplitudes.

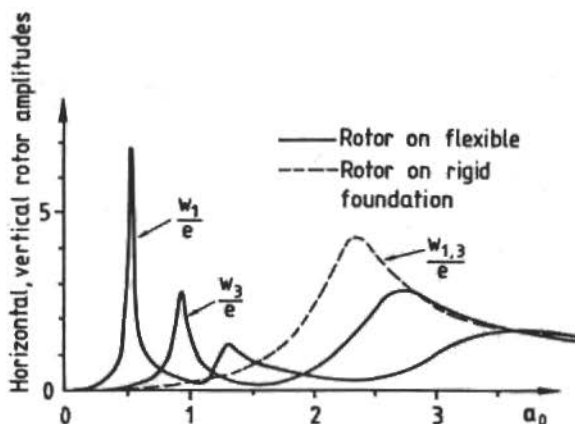


Figure 15. Response of Laval rotor and rigid and flexible block foundation

Turbomachinery Frame Foundation Supported by Piles

Aboul-Ella and Noval 1978 analyzed the dynamic response of turbomachinery frame foundations supported by piles or a foundation slab. Their study investigates interaction of all components of the system, i.e. flexible rotors, viscoelastic oil film, space frame, flexible mat piles and soil (Fig. 16). The mat is composed of rectangular finite plate elements. The pile and soil resistance is included into mat element stiffness matrix. The dynamic complex soil stiffness matrix is obtained from Gual (1977).

In the study of Aboul-Ella and Novak special attention is paid to the effects of soil-structure interaction. It was found that this interaction markedly affects the response of the frame as well as the rotors in the lowest resonant regions. The interaction reduces rotor and frame amplitudes. This results from the increase in damping due to energy radiation in the soil and viscoelastic behaviour of soil and mat. The interaction reduces

the frame vibration more than shaft vibration..

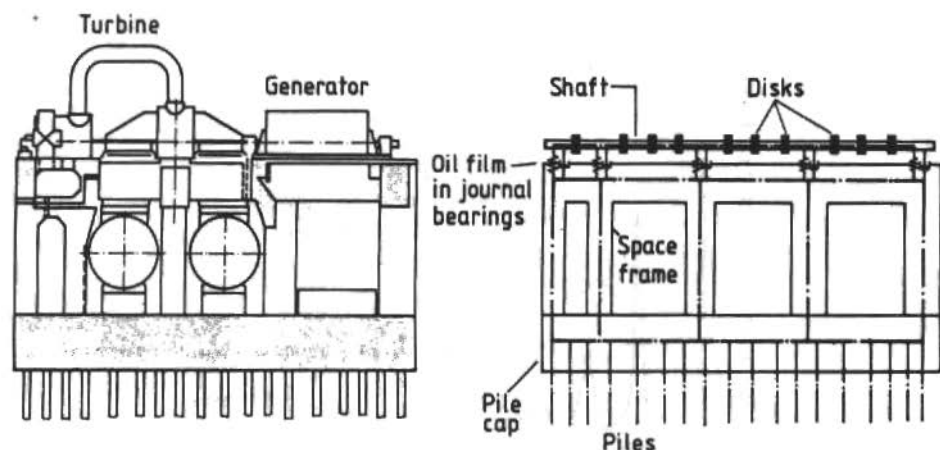


Figure 16. Turbomachinery frame foundation and its model

E.g. Fig. 17 compares the vertical response of frame under bearing pedestal corresponding to a rotor on elastic frame and rigid foundation with a rotor on elastic frame and elastic foundation.

EXPERIMENTAL INVESTIGATION OF SOIL-STRUCTURE INTERACTION

Measured Response of a Model Frame Foundation

The response of a frame foundation according to the model of Fig. 10 was simulated by a small scale model (Fig. 18). Four rotating unbalances driven via a control gear allow for coupled and uncoupled excitation by horizontal and vertical forces and by torsion and rocking moments. The stiffness of coupling between upper plate and base plate can be varied by changeable columns. Rubber springs simulate the soil.

The sine sweep response of 12 degrees of freedom were measured by velocity pick-ups. The results are in good agreement with those calculated by Eqs. (16) to (21) (Gaul, Mahrenholtz 1981).

The coupled horizontal and rocking modes in Fig. 19 correspond to the calculated modes in Fig. 14.

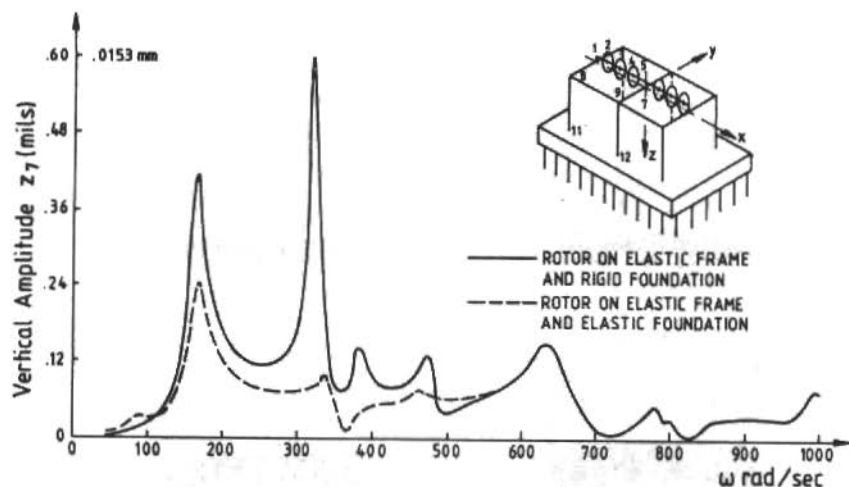


Figure 17. Effect of foundation (piles and soil) flexibility on vertical response of frame under bearing pedestal

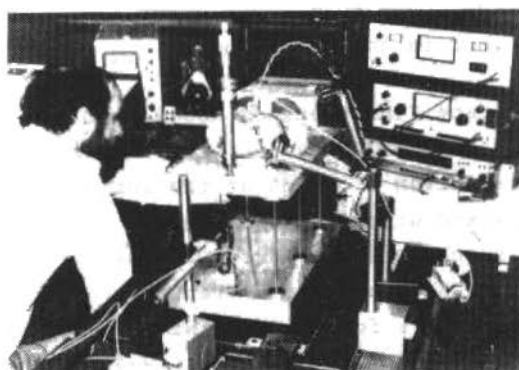


Figure 18. Small scale model of frame foundation with measuring setup

Level Shaft on a Model Frame Foundation

For simulating the interaction between rotating shaft, frame foundation and subsoil on a model scale, the lab model of Fig. 20 has been built. A laval shaft with adjustable disk position and excentricity driven by a variable speed motor is supported by two ball-bearings on the upper foundation plate.

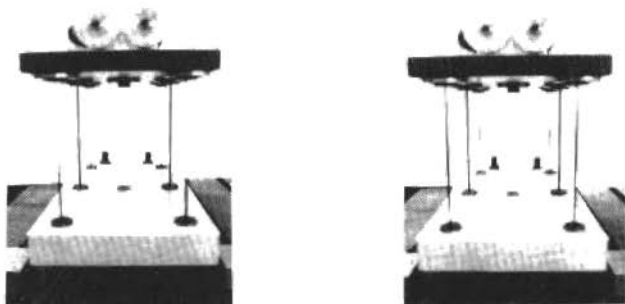


Figure 19. Vibration modes of frame foundation on rubber springs

The experimental work in progress simulates the interaction effects of the three substructure where the base plate is bedded on rubber springs, on a foam layer or on a model sand foundation which is explained in the next chapter.

Steady-State Vibrations of Model Footings

The substructure behaviour of soil was measured on a model scale by shaker-driven footings at the surface of homogeneous or layered sand mixed with gravel (Fig. 21). The response of acceleration and phase angle versus frequency of the sine sweep (Fig. 22) as well as the deduced frequency dependent lumped parameters of soil are found in satisfactory agreement with calculated results (Gaul, Mahrenholtz 1984).

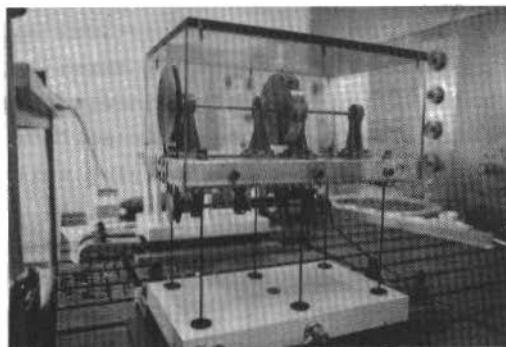


Figure 20. Lab model for measuring interaction effects between rotating shaft, frame foundation and subsoil

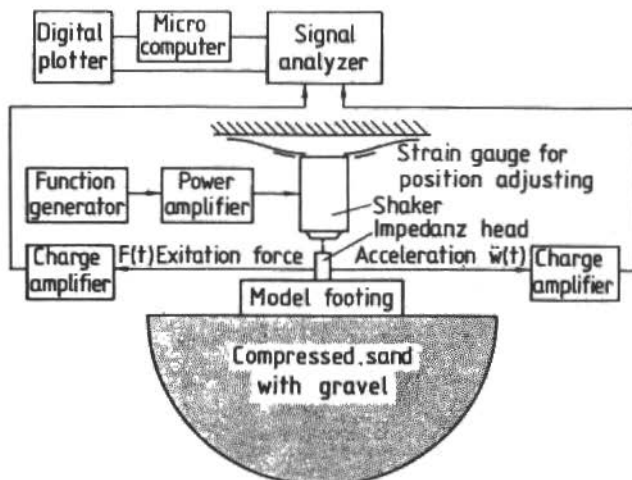
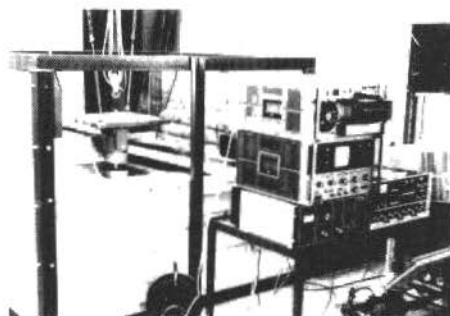


Figure 21. Experimental setup of shaker-driven model footing

SUMMARY AND CONCLUSIONS

On the basis of substructuring a theoretical approach has been formulated and programmed to analyze the three-dimensional dynamic response of machine foundations considering the interaction of the system components; namely, viscoelastic soil, frame and rotor, as well as the interaction through the underlying soil with an adjacent structure. Geometrical as well as material damping of soil are considered. Material damping is found to be of considerable influence for rocking motion. The influence of shear stresses at the interface between base and soil is limited. It makes little difference whether the contact at the interface is smooth or welded. The dynamic response of a model frame foundation and a model footing on compressed sand are measured. Both, theoretical approach and experiments, provide a good understanding of the basic interaction effects.

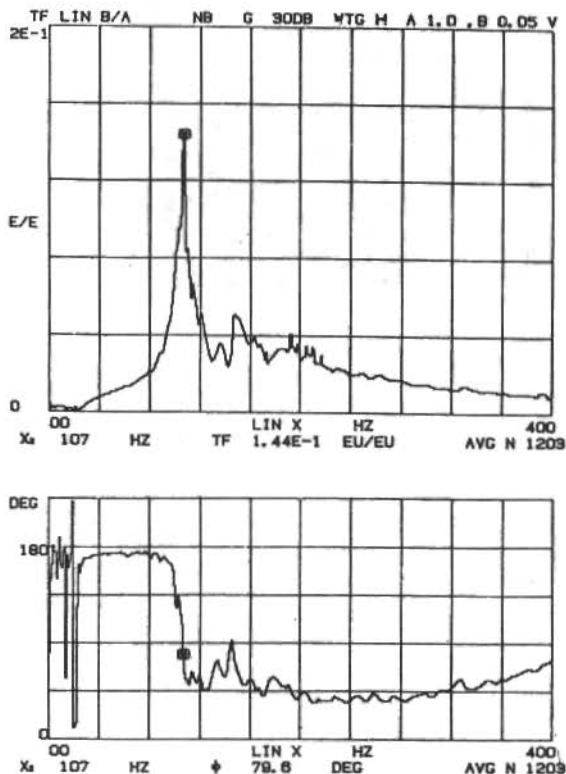


Figure 22. Sine sweep response of vertical vibration for a circular model footing

ACKNOWLEDGMENTS

The experimental research with model footings performed by Dipl.-Ing. M. Plenge, University of Hanover, is gratefully acknowledged.

This study was supported by the Deutsche Forschungsgemeinschaft (German research council).

REFERENCES

- [1] Aboul-Ella, F.A. & M. Novak 1978. Dynamic analysis of turbine-generator foundations. Presented at the 1978 Fall Convention, Houston, Tex., Oct.
- [2] Aboul-Ella, F.A. & M. Novak 1980. Dynamic response of pile - supported frame foundations. Journal of the Engineering Mechanics Division, Proc. ASCE, Vol. 106, Nº EM6, Dec., pp. 1215-1232.
- [3] Almansi, E., 1907. Un Teorema Sulle Deformazioni Elastiche dei Solidi Isotropi, Atti della reale accademia dei nazionale Lincei, Vol. 16, pp. 865-868.
- [4] Crandall, S.H., Kurzweil, L.G. & A.K. Nigam 1971. On the measurement of Poisson's ratio for modeling clay. Experimental Mechanics, 11, pp. 402-407.
- [5] Dasgupta, G., 1979. Wellposedness of Substructure Deletion Formulations. Proceedings, Sixteenth Midwestern Mechanics Conference, Vol. 10, Manhattan, Kansas.
- [6] Dasgupta, G., 1980. Foundation Impedance Matrices by Substructure Deletion. Journal of the Engineering Mechanics Division, American Society of Civil Engineers, Vol. 106, nº EM3, pp. 517-523.
- [7] Dietz, H. 1972. Stahlfundamente für Turbomaschinen. Beratungsstelle für Stahlverwendung, Düsseldorf, Merkblatt 146,3.
- [8] Gasch, R & W Sarfeld 1980. Unwuchterzogene Schwingungen des Systems LavalläuferBlockfundament - elastischer Halbraum, VDI-Berichte Nr. 381, pp. 129-138.
- [9] Gaul, L. 1977. Dynamische Wechselwirkung eines Fundamentes mit dem viskoelastischen Halbraum. Ing.-Archiv, 46, pp. 401-422.
- [10] Gaul, L. 1980. Zur Dynamik der Wechselwirkung von Strukturen mit dem Baugrund. Habil. Univ. Hannover, June.

- [11] Gaul, L. 1980a. Dynamics of frame foundations interacting with soil. *Journal of Mechanical Design*, Vol. 102, pp. 303-310.
- [12] Gaul, L. & O. Mahrenholtz 1981, 1984. Dynamischewechselwirkung zwischen Maschine, Fundament und Baugrund. Arbeitsbericht zum DFG-Schwerpunktprogramm Betriebsverhalten dynamisch belasteter Maschinen (not published).
- [13] Gaul, L. & M. Plenge 1983. Ein Baugrundmodell für geschichtete Baugründe mit viskoelastischem Stoffverhalten. *ZAMM* 63, pp. T50 - T53.
- [14] Holzlöhner, U. 1969. Schwingungen des elastischen Halbraumes bei Erregung auf einer Rechteckfläche. *Ing.-Archiv*, 18, pp. 370-379.
- [15] Huh, Y, Schmid, G. & M. Ottenstreuer 1983. Evaluation of kinematic interaction of soil-foundation systems by boundary element method. *SMIRT 7 Chicago*, August, Paper K814.
- [16] Knobloch, W. & L. Gaul 1975. Dämpfungs- und Federverhalten elastischer und viskoelastischer Gründungen bei harmonischer Erregung. *Kolloq. Viskoelastische Systeme, VDI-GKE, TU Berlin*, pp. 412-451.
- [17] Krämer, E. 1984. *Maschinendynamik*. Springer Verlag Berlin.
- [18] Novak, M. 1982. Response of hammer foundations. *Proc. soil dynamics and earth-quake engineering conference Southampton*, July, pp. 783-797.
- [19] Ottenstreuer, M. 1982. Frequency dependent dynamic response of footings. *Proc. soil dynamics and earthquake engineering conference Southampton*, July, pp. 799-809.
- [20] Sarfeld, W. & C. Fröhlich 1980. Dynamische Wechselwirkung von Gebäuden und Fundamenten auf dem elastisch-isotropen Halbraum, *Bauingenieur* 55, pp. 419-426.
- [21] Thurat, B. 1978. *Maschine-Fundament-Baugrund*. Diss. RWTH-Aachen.
- [22] Waas, G. 1972. Linear two-dimensional analysis of soil dynamics problems in semi-infinite layered media, Ph.D. Thesis, University of California, Berkeley.

TOWARD THE UTILIZATION OF COMPUTER INTELLIGENCE IN METAL MACHINING

Dr. Hejat Olgac

University of Connecticut - USA

ABSTRACT

Very difficult task of coordinating controllable parameters of metal cutting needs a lengthy experience of human operators. The accumulated knowledge in the minds of expert machinists can now be delivered - at least partially - to the intelligent controllers of such equipment as CNC Lathes, milling machines, drills, etc. The sensory feedback control structure which is often times referred as "Adaptive Machine Tool Control Set-up" is addressed in this work.

The principle aim of this study is to achieve the two important steps of the Adaptive Control System (ACS). One is to successfully gather the necessary pieces of information about the ongoing dynamic event. And the second is to process this dynamic data in real-time in order to generate the commands which would otherwise be introduced by the expert machinist. So the goals can be renamed as sensing and control respectively.

Normally the signature of any dynamic data brings a stochastic feature to the problem we just posed. The study entails the treatise of such complex data structures, by using an off-line "learning" or "adaptation" package to be introduced to the real time operator. A typical lathe cutting operation is chosen as the generic application case. Various findings of the experimental work and critical points of monitoring the dynamic behavior are discussed along with the future research directions on this control operation.

INTRODUCTION

The influence of computers in manufacturing operations is reaching for broader application areas everyday. The novel uses computerized process control operations become routine tasks as new techniques are developed, and the "unthinkables" are becoming closer to the reach of the human race [1]. What governs this rapid enhancement in the technology is the astonishing strength of the microprocessors' world. The more powerful chips, the better computers, the faster performing software naturally result in perfectly desirable environment for the production operation. In this report the intension is to cover a broad range of computerized manufacturing problems, with the state-of-the art issues and future trends, research topics as well as the difficulties encountered in the direction of intelligent/smart operations.

It should be underlined that although it looks as if the forerunning scientists are trying to achieve the age of human replicas, it is not the case from various perspectives [2]. First of all the combined perfection of sensory capabilities of human beings is impossibility difficult to duplicate. Therefore, very limited sensory interaction can be aimed between the "autonomous devices" and their environments. Secondly, the speed and sophistication of human brain are rather difficult to obtain via electronic components. This issue is a very important one from the point of making observations, recognitions and controls in real-time (i.e. while the events actually proceed in their dynamic structures). What it is, then, which makes the scientists strive for achieving, is the importation of computerized schemes into various traditional "skilled labor" operations. The reason for this, as well known, is "the advantage of the repeatability and the storage potential of the computerized operations".

A significant breakthrough in the computers involvement in manufacturing comes in design: CAD (Computer Aided Design), CAG (Computer Assisted Graphics). Even in the 3-Dimensional (3-D) sense, design is a routine activity for the computer users today. Another facet in which computerization assisted the manufacturing operations is, naturally, CAM (Computer Aided Manufacturing) or CIM (Computer Integrated Manufacturing). In this report we look into the marriage of CAD and CAM in an autonomous. The word "autonomous"

is rather controversial one. Our use in this text covers the features of "on-line decision generations without a supervisory triggering based on a set of sensory understanding of the dynamics state".

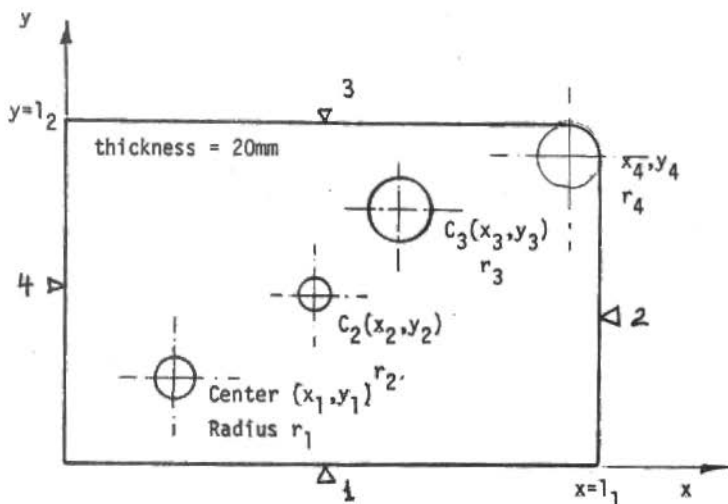
In the center of our discussions a typical orthogonal lathe cutting process is taken for its very descriptive nature [3-6]. The above mentioned autonomous control directions are defined, along with the sensory bases for these decisions. The difficult task of interpreting the signals from the sensors in very short time intervals are discussed. This interpretation naturally represents the form in which the controller is informed about the status of the process (i.e. this is the feedback data).

There are two fundamental techniques of manipulating the above mentioned data; FFT (Fast Fourier Transformation Analysis) and ARMA (Auto Regressive Moving Average Method) [7]. The nature of the control actions are described in response to the data feedback. Even in the chosen simple cutting conditions, these observation data is noisy enough to call for a stochastic treatment.

A particular conception of stability in the machining operations is expressed. The primary concern of the controller is to assume the "stable" operating conditions as well as those of "optimal". Since there are fundamental dynamic changes in governing equations of the process, this operation is often times referred to as "Adaptive Control with Optimization" [6].

CAD/CAM IN THE PERSPECTIVE OF "AUTOMATIC CONTROLS"

A successful coupling of CAD with CAM can be named a priori defined/programmed and partially feedback type control systematic. "A Priori" because the programmer defines the shape of the final product, the starting primitive workpiece, the cutting tool paths (in the case of machining) to the level of machine language. In Figure 1a self descriptive program for a 2-D machining process is depicted. There are many tool path generating packages today which are commercially available. They simply need the 3-D graphics (such as Figure 1b) descriptions of the parts to be manufactured and the starting primitives [8]. That is, the leg from the graphics to the machine code is autonomous (i.e. it is handled without the need of a human supervision).



Hole no 1: with tool no 1, speed ω_1
 Hole no 2: with tool no 2, speed ω_2
 Hole no 3: with tool no 3, speed ω_3

Surface 1 and 4 with tool A and speed ω_a
 Surface 2 and 3 with tool B and speed ω_b

Figure 1a. 2-D representation of a part with CNC programming instructions

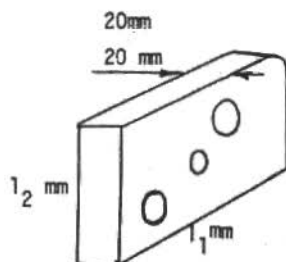


Figure 1b. The 3-D representation of the same object

But there is an important - and again a priori - guidance based on operator and/or programmer experience which goes into this path program. It is the set of specifications of the step by step operation:

- the tools to be used for each segment of the process;
- the operating speeds at each and every point of the process;
- if used the volume of cutting fluid and variety (if there exists different types);
- the ways in which the workpiece is to be secured to the operation platform, etc...

For instance if an array of tools are involved as shown in Figure 2 their positions on the tool rack should also be specified. In other words a computerized manufacturing process in this sense, has to have full guidance of the operator/programmer sketched out even before the operation starts. Naturally without the knowledge of instantaneous, unexpected, on-line abnormalities. If all goes as predicted the program successfully proceeds and materializes the ultimate goal. But, what happens if a sudden tool breakage takes place, or a segregated material abnormality exists...? Is the computerized controller prepared to take proper action in order to compensate for such array of "on-line" events? Just based on this question the CAM operations can be grouped into two major categories:

- a) A priori programmed, off-line CAM operation.
- b) On-line, autonomous CAM operations.

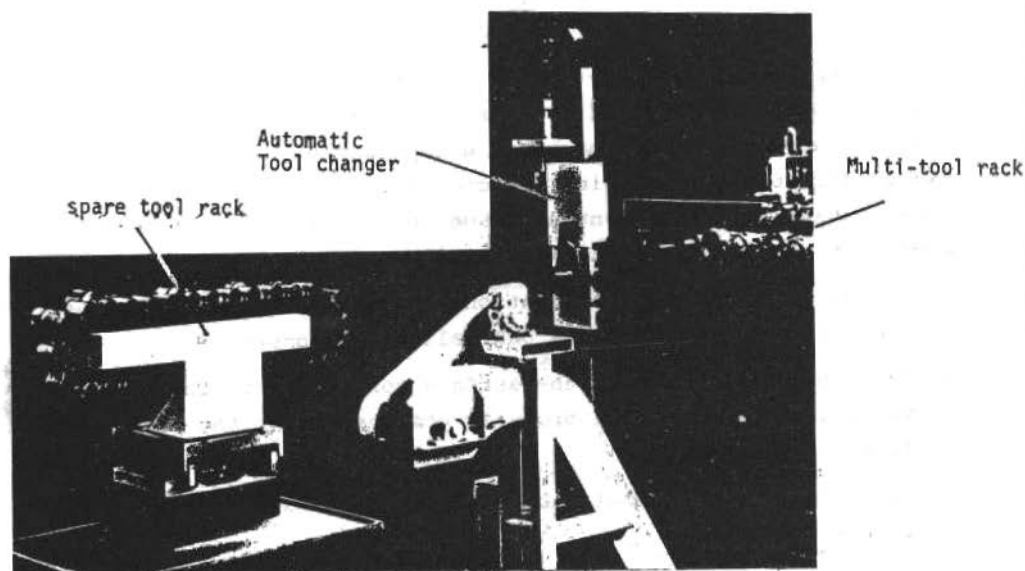


Figure 2. A typical tool rack with coded tools
(from Cincinnati Milacron FMS set-ups)

In principle, the first category entails the multi-axes motion control operations. A few examples may be listed as:

- moving the pens on a color plotter, without checking the ink level in the pens;
- guiding a robot arm without questioning whether the liquid being transported is spilled or the orientation of the object to be manipulated is not as originally planned;
- metal machining without continuously monitoring the tool forces, as it is in the framework of the main stream-line of this report.

This list can be expanded much beyond the limits of a CNC (Computerized Numerical Controlled) machining operations as seen from the variety of examples. All of them have some common features:

1. All are targeting certain multi-axial motion coordination.
2. All are a priori programmed and they are partially feedback as indicated earlier. Figure 3 depicts a small closed loop control over the position of a machine tool cutter.

The second category of cam operations, which is the central element to the research efforts in these days, entails the struggle toward generating "smart machine" equipped with a "brain" of their own by effectively utilizing the computer intelligence. This constitutes the quintessential issue in this work. A few typical questions that arise in metal machining processes are:

1. How can the tool tip oscillations (possibly the undesirable event called "chatter") be controlled autonomously?
2. Can the machine monitor the surface conditions of the sections which are being cut and properly compensate for the undesired level of roughness?
3. Can a sense of "optimal machining" be introduced in the operation? etc...

These questions and alike lead us toward an operating scheme of the future covering two basic issues:

1. An intelligent, on-line recognition of the working environment

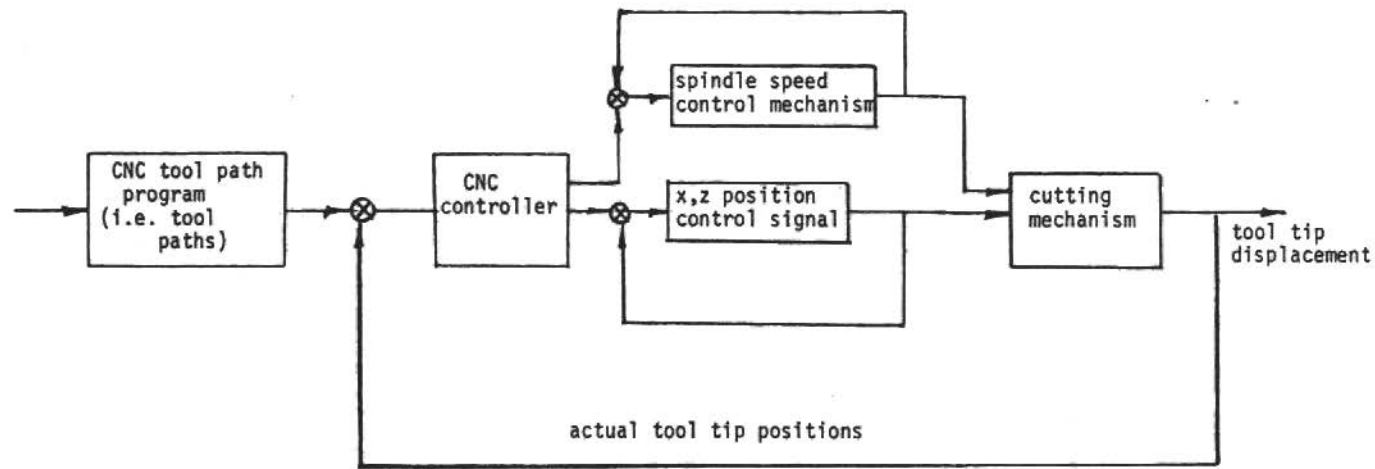


Figure 3. Partially closed loop machining for the position of the tool tip

by the machines via sensory devices (e.g. vision, touch sensing, position-speed-acceleration sensing, etc.).

2. A sophisticated, algorithmic machine logic in order to comprehend the sensory information developed in (1) and judge for the control actions. That is, a higher echelon of feedback control systematic or sometimes an "adaptive control".

The following segments of this report address these line items in the framework of metal cutting. But, again, it should be understood that the treatment is general enough to be applied to much larger group of "smart operations" beyond metal cutting systems. Simply, the availability of the accumulated expertise of machining process makes it a good candidate to elaborate on.

AN APPLICATION PROBLEM: METAL CUTTING PROCESS ON A LATHE

An orthogonal turning process is depicted in Figure 4, with the basic parametric quantities. The structural support elements k 's and b 's represent the spring stiffness and structural damping features of the tool holding set-up. The cutting forces at the tool tip vs. workpiece interface are also shown.

On this general 3-D lathe cutting mechanism a computerized "smart" control operation can be stated as follows:

1. Assume that the process is controlled by the decisions on three quantities:
 - a. The spindle speed of the lathe chuck, ω (RPM)
 - b. The feed rate of the tool-bit, f (mm/sec)
 - c. The depth of cut variations, d (mm)

These elements can be controlled via servomotor (or for practical experiments stepping motor) drive mechanisms. Figure 5 depicts a lathe with the control actuating drive motors.

2. A sensory device: a 3-D dynamometer is utilized to monitor the 3-D force and displacement variations at the tool tip. As shown in Figure 6 this sensing set-up is equipped with 3 LVDT's (Linear Variable Differential Transducers) which produce the signature of the displacements generated at the tool holder. These signatures in turn represent a set of force variations in the corresponding directions (i.e. the cutting, thrust and feed

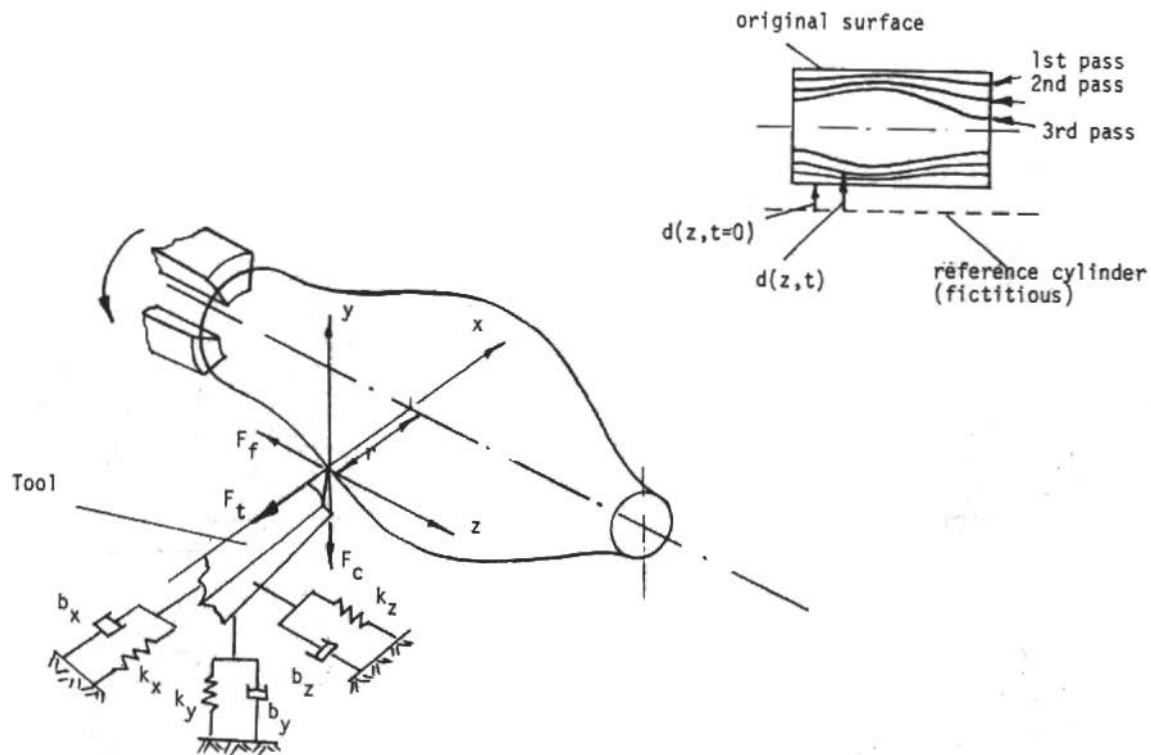


Figure 4. Typical lathe cutting mechanism, with tool forces

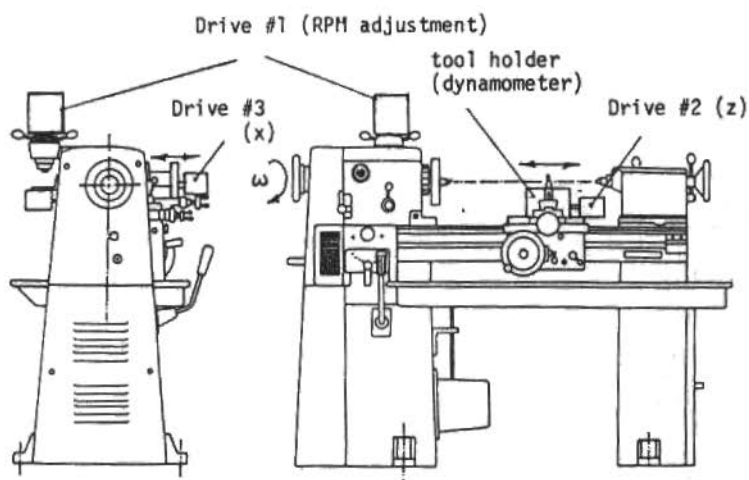


Figure 5. A typical lathe with speed and (x,z) position control drives

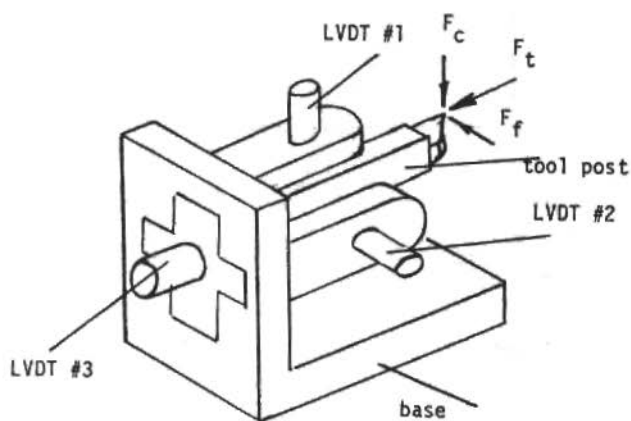


Figure 6. The schematic of the dynamometer

forces). Note that a linear relationships between these forces F_c , F_t , and F_f (respectively) vs. the tool tip displacements u , v , w are assumed. Therefore the operation in hand is in "elastic zone" for the purposes of simplification. Indeed if any plastic deformation takes place the concept of precision cutting will be terribly risked. Therefore the relationship between the forces and the displacements can be stated as:

$$\begin{bmatrix} F_t \\ F_c \\ F_f \end{bmatrix} = \begin{bmatrix} \alpha_{11} & \alpha_{12} & \alpha_{13} \\ \alpha_{21} & \alpha_{22} & \alpha_{23} \\ \alpha_{31} & \alpha_{32} & \alpha_{33} \end{bmatrix} \begin{bmatrix} u \\ v \\ w \end{bmatrix} = A \begin{bmatrix} u \\ v \\ w \end{bmatrix} \quad (1)$$

where α_{11} , α_{22} , α_{33} are the direct influence coefficients while α_{ij} ($i \neq j$) are the cross coupling between the directions. The matrix (A) is determined experimentally and assumed constant after the initial calibration of LVDT's.

3. The fundamental problem is: How can the above described sensing (feedback) and control systematic operate to achieve an optimal machining? The optimality can be defined in different formats. For the coverage of this report we pursue with:
- maximizing the metal removal rate, i.e.

$$\max r \omega(t) b(d, f, t) d(t) = v \text{ (mm}^3/\text{sec)} \quad \text{Figure 7} \quad (2)$$

(ω, d, f)

- with a bounded tool force structure

$$\begin{aligned} F_t(t) &\leq F_{t, \max} \\ F_c(t) &\leq F_{c, \max} \\ F_f(t) &\leq F_{f, \max} \end{aligned} \quad (3)$$

- for a dynamic system which is implicitly described as:

$$F(F_t, F_c, F_f, \omega, d, f, t) = 0 \quad (4)$$

- And the ultimate goal is to achieve a geometry shown in

Figure 4. That is from $d(z, t = 0) = 0$ (the initial shape of the piece), to $d(z, t = t_f)$ (the final shape of the piece) where

t = time (sec)
 t_f = final time (sec)
 $r\omega(t)$ = linear cutting speed (mm/sec)
 $\omega(t)$ = angular speed of the spindle (rad/sec)

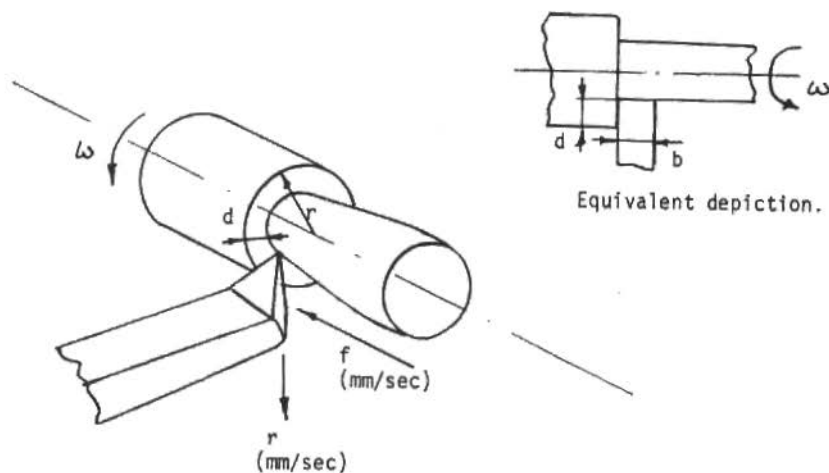


Figure 7. The depiction of the metal removal rate

This optimization problem is a very complicated one, due to the lack of a sufficiently precise state equation (4). An analytical model relating the control parameters (ω, d, f) to the tool forces (F_t, F_c, F_f) has been the subject of many research programs. Unfortunately there is no unified and precise analytical representation which fits the general turning mechanism. This is fundamentally because of an extraordinarily large number of parameters which do not appear in eq. (4) but have strong influence on the dynamic structure. For instance the tool sharpness, rake angle, clearance, chip forming notch geometry, etc. In the presence of a very obscure relationship of this nature the solution to the problem stated in eq.'s (2-4) becomes extremely difficult. This report focuses on a solution technique and suggests an extension as a further research project.

AN ADAPTIVE CONTROL VIA PROPORTIONAL FEEDBACK

The optimization problem as stated in equations (2-4) has some extra constraints which are not included in the mathematical formulation. First set of these constraints is about the "positive cutting" (i.e. cutting with continuous removing of material). Simply

$$\begin{aligned} v(t) &\geq 0 \\ d(t) &\geq 0 \quad \text{at all times } 0 \leq t \leq t_f \\ f(t) &\geq 0 \end{aligned} \quad (5)$$

should be satisfied. Additionally the system capabilities become limiting factors. Such as:

$$\begin{aligned} \omega(t) &\leq \omega_{\max}, \quad \left. \frac{d\omega(t)}{dt} \leq \frac{d\omega}{dt} \right|_{\max} && \text{spindle speed and its} \\ & && \text{time rate of change} \\ d(t) &\leq d_{\max}, \quad \left. \frac{dd(t)}{dt} \leq \frac{dd}{dt} \right|_{\max} && \text{the depth and its time} \\ & && \text{rate of change} \\ f(t) &\leq f_{\max}, \quad \left. \frac{df(t)}{dt} \leq \frac{df}{dt} \right|_{\max} && \text{the feed rate and its} \\ & && \text{time rate of change} \end{aligned} \quad (6)$$

Noting that although an analytical representation is not available the implicit relationship of (4) has all positive gradient vector scalar products in the ω, d, f space (Figure 8). That is the matrix

$$\begin{bmatrix} \frac{\partial F}{\partial F_t} \\ \frac{\partial F}{\partial F_C} \\ \frac{\partial F}{\partial F_f} \end{bmatrix} \begin{bmatrix} \frac{\partial F}{\partial \omega} & \frac{\partial F}{\partial d} & \frac{\partial F}{\partial t} \end{bmatrix} = (\nabla F)_{F_t, F_C, F_f}^T \cdot (\nabla F)_{\omega, d, t} \quad (7)$$

has all positive components. Because if any one of the control parameters ω, d, t were increased ($d\omega$ or dd or $dt > 0$) the force components would increase. Therefore, dF_t or dF_d or $dF_t > 0$ corresponding to the increases are expected intuitively, as well as the objective function indicated in (2)

$$\frac{\partial v}{\partial \omega} \geq 0, \quad \frac{\partial v}{\partial d} \geq 0, \quad \frac{\partial v}{\partial f} \geq 0 \quad \text{i.e. } \nabla v \geq 0 \quad (8)$$

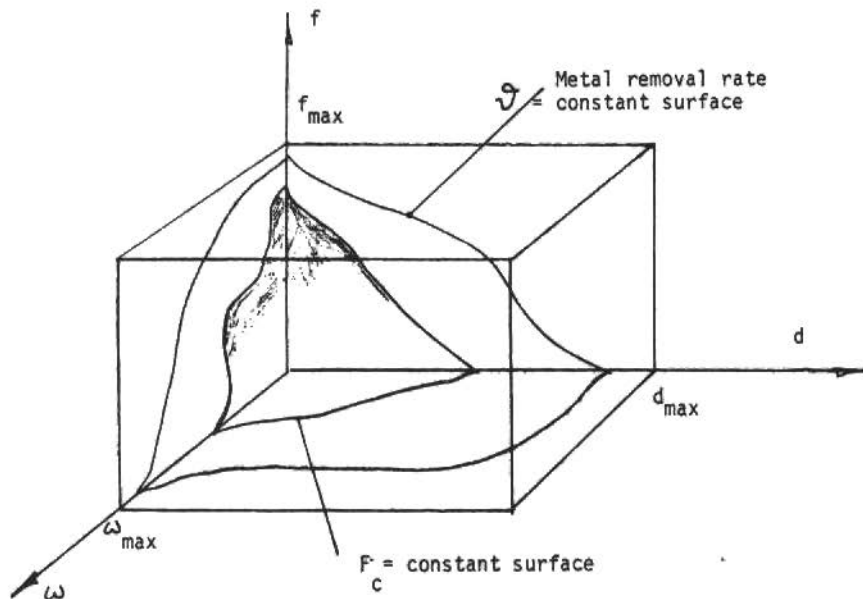


Figure 8. The constraints in ω, d, f domain with fixed force and metal removal rate surfaces

Since the v is to be maximized the steepest possible gradient direction is to be followed as the optimal path, naturally without violating the constraints (3, 5 and 6). For the sake of simplicity in the following portion of discussions we worry about only one force (instead of three) let's say the cutting force $F_c(t)$.

The equation (4) can be rewritten as:

$$F_c = F_c(\omega, d, f, t) \quad (9)$$

The constant F_c curves in the ω, d, f space (Figure 8) also have positive gradients, following equation (7).

$$\frac{\partial F_c}{\partial \omega} \geq 0, \quad \frac{\partial F_c}{\partial d} \geq 0, \quad \frac{\partial F_c}{\partial f} \geq 0 \quad \text{i.e.} \quad \nabla F_c \geq 0 \quad (10)$$

The optimal operating conditions are located on the surface described by

$$F_c(\omega, d, f, t) = F_{c, \max} \quad (\text{see Figure 9}) \quad (11)$$

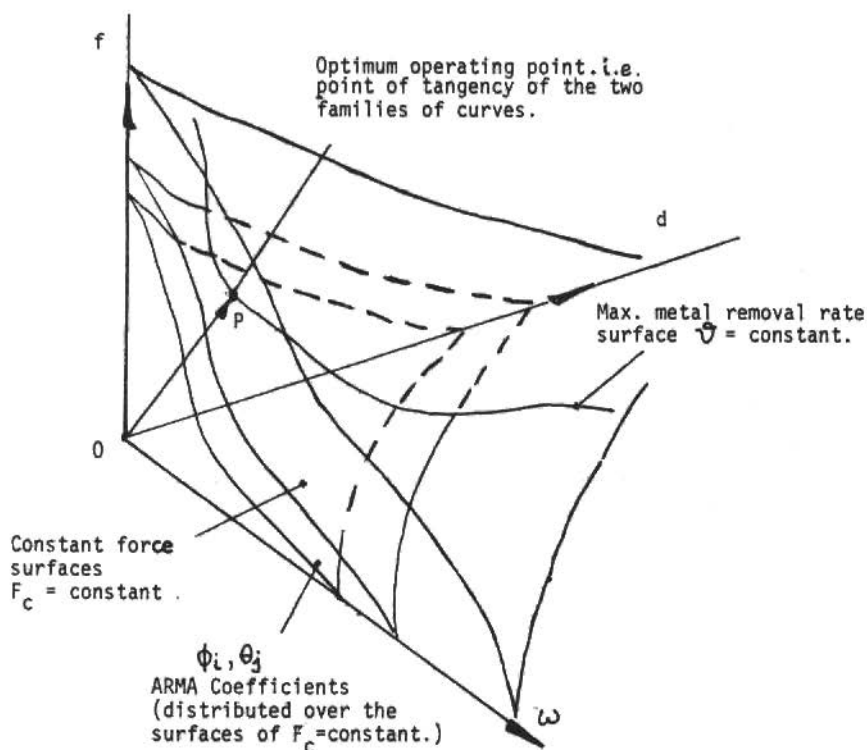


Figure 9. $F_c = \text{constant}$ and $v = \text{constant}$ curves with optimal operating point

The optimal direction is determined, which is OP. The control system should guide itself toward point P, by varying the parametric cutting quantities (ω , d and f), and stay there throughout the cutting process.

A few difficulties arise at this point. First, the functional relationship (9) is not explicitly given, consequently the optimal point P is not well defined. On the other hand the family of curves with

$$F_c(\omega, d, f, t) = \text{constant}$$

can be obtained through the experiments. Then, these practical results are used to find point P. Since the optimal direction of operation is known the problem seems to be solved.

The second difficulty is to compensate for unexpected cutting force variations. For instance, a segregated hardness on the surface or a corner type profile change may cause these and therefore introducing a departure from the $F_c(\omega, d, f, t) = \text{constant}$ surface. Since this type of dynamics is changing the system characteristics, the remedial control systematic is to be "Adaptive". A proportional feedback adaptive control loop is depicted in Figure 10 in a very simple format.

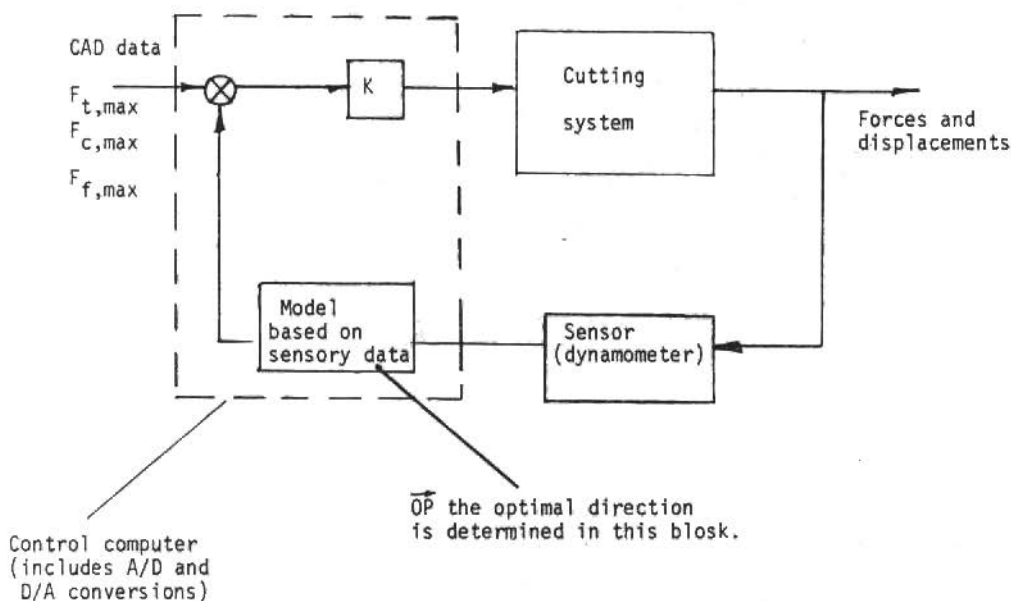


Figure 10. Typical force-limiting-adaptive control loop systematic

Figures 11 and 12 represent two experimental results. Note that in Figure 12 the sudden departure from constant F_c surface takes place and an immediate adaptation is taken by the controller (in this case directly through reducing d , i.e. single input-single output adaptive control). In Figure 11 on the other hand the expected smooth force variation is reached at the $F_i = F_{c,max}$ level.

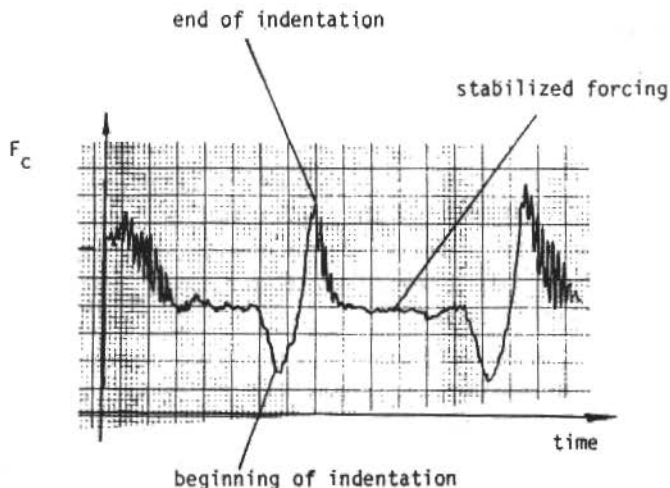


Figure 11. The cutting force variation in the case of disturbing surface indentation

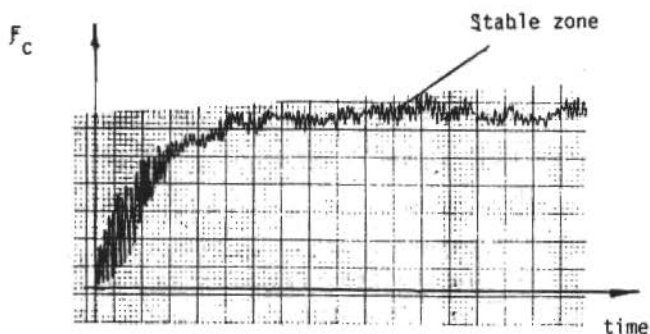


Figure 12. The cutting force on a smooth surface

The entire control operation is governed via a digital computer which has analogue to digital (A/D) and Digital to Analogue (D/A) conversion capabilities (Figure 10). The time element becomes very important in this operation in the "on-line control" situation. The "smart machine" is in hand, but the speed should be enhanced to the level in which the control actuations can be manipulated in a timely manner. As we approach toward higher speed machining this problem becomes a more substantial one. This question is under investigation by a group including the author.

FUTURE RESEARCH DIRECTIONS AND FORECASTING

Being aware of the above mentioned difficulties the following problem formulation is suggested in a parallelism to [8]. Given the optimal control problem of equations (2-10) is there an on-line method which will enable the controller to forecast the onset of the future states? The answer to this question is "no". But, if we consider that for some given ω , d and f with the other cutting parameters fixed, a data-base force signature $F_C(t)$ registration and forecasting can be made.

The method named ARMA (auto regressive moving average) is utilized in such an effort [9] where the $F_C(t)$ vs. t data registrations with variety of ω , d , f points are made. For each one of these points a discrete time linear Stochastic model is found following [10] in the form of ARMA (n,m)

$$F_C(t) - \phi_1 F_C(t-1) - \phi_2 F_C(t-2) - \dots - \phi_n F_C(t-n) = a(t) - \theta_1 a(t-1) - \theta_2 a(t-2) \dots - \theta_m a(t-m) \quad (12)$$

where

$F_C(t-i)$: the force measurement at the time $t-i(\Delta t)$

Δt : the time interval of force measurement

ϕ_i : Auto Regression Coefficients

$a(t-i)$: normally, independently distributed (NID) moving average parameter at time $t-i(\Delta t)$. This term represents the stochastic variation between the actual and calculated (via equation 12) $F_C(t-i\Delta t)$ values.

θ_i : moving average coefficients

n : the degree of auto regression

m : the degree of moving average

The equation (12) is an iterative one if ϕ_i , θ_j 's are known and the first n data points from $t-n$ to $t-1$ are registered. Consequently $F_C(t)$, $F_C(t+1)$... can be calculated provided that the other system parameters (such as ω , d , f , etc.) are all kept unchanged.

The important point in (12) is that the $n+m$ coefficients ϕ_i and θ_j 's should be calculated based on the largest possible data preferably off-line and prior to the actual controlled cutting process. So, as Figure 9 indicates there exists a descriptive set of ϕ_i and θ_j 's for each and every point in the ω, d, f space (i.e. a library of ϕ 's and θ 's).

Being equipped with the ARMA (n,m) coefficient library the dynamic characteristics of $F_c(t,\omega,d,f)$ can now be predicted on-line and the direction of optimally as described in the previous section can be enhanced under the light of the knowledge of the future state values.

There are number of problems associated with the proposed line:

1. To establish a large library of coefficients ϕ_i, θ_j 's for individual points in ω, d, f space. Note that this is an off-line process.
2. To rapidly search for the appropriate ϕ_i, θ_j 's for a given F_c registration in real-time (which is a very difficult task to handle).
3. To develop the decisions over the control parameters ω, d and f (as defined earlier) and implement them.
4. To continue the rapid data registrations for the next step of control application..

These 4 items have different faucets of research arenas of their own. Author's group and various others are currently pursuing these lines. The most important issue is to develop a systematic which is simple enough to employ in real-time, an yet sufficiently sophisticated to address all types of possible sensor signatures.

ACKNOWLEDGEMENT

Author wishes to acknowledge the financial support from the National Science Foundation via the grant numbered NSF MEA 8300236 which made the studies on some of the above mentioned issues possible. At the least sincere thanks are due for the University of Connecticut, Mechanical Engineering Department staff and machine shop personnel for their assistance and Mrs. Joanne Moore for her determined efforts in typing this manuscript.

REFERENCES

- [1] Mitchell, R.K. - Involvement and integration - A Route to CAD/CAM. Mechanical Engineering, June 1985.
- [2] Edson, D.V. - Giving robot hands a human touch. High Technology, September 1985.
- [3] Olgac, N. and Devin, M. - A study on the computer modelling of the lathe cutting mechanism. International Journal of Modeling and Simulation, March 1984.
- [4] Boothroyd, G. - Fundamentals of metal machining and machine tools. McGraw-Hill (1975).
- [5] Tobias, S.A. - Machine tool vibration. Wiley (1975).
- [6] Ulsoy, A.G.; Koren, Y. and Rasmussen, F. - Principle developments in the adaptive control of machine tools. ASME Trans., J. of Dynamic Systems, Measurement and Control, v.105, June 1983.
- [7] Eman, K.F. and Wu, S.M. - Forecasting control of machining chatter. The Winter Annual Meeting of ASME, Chicago, November 1980.
- [8] Olgac, N. and Kazerounian, K. - Development of smart algorithms for on-line-optimal control of computer integrated systems, a grant proposal to the federal agencies. University of Connecticut, September 1985.
- [9] Olgac, N. and Guoquan, Z. - A computer modelling study for the general turning mechanisms. to appear.
- [10] Wu, S.M. and Pandit, S.M. - Time series and system analysis, modelling and application. John Wiley (1983).

SOBRE A INTERPRETAÇÃO DO TENSOR PARCIAL DE TENSÃO E DA FORÇA DIFUSIVA EM MISTURAS SÓLIDO-FLUIDO

Rogério Martins Saldanha da Gama - Membro da ABCM

LNCC/CNPq

Rubens Sampaio - Membro da ABCM

DEM-PUC/RJ

RESUMO

Neste trabalho procura-se, através de exemplos simples, apresentar uma interpretação física para alguns elementos que surgem naturalmente na análise de fenômenos físicos, sob o ponto de vista da Teoria Contínua de Misturas. Aqui buscamos as interpretações partindo da Mecânica dos Meios Contínuos Clássica e chegando até a Teoria de Misturas.

ABSTRACT

On the Physical Interpretation of the Partial Stress Tensor and Diffusive Force in Solid-Fluid Mixtures.

In this work we are interested, through simple examples, in showing a physical interpretation for some elements that arise naturally in the analysis of physical phenomena under the Continuum Theory of Mixtures viewpoint. Here we take the interpretations going from Classical Continuum Mechanics to Theory of Mixtures.

INTRODUÇÃO

Quando um fluido escoar através de um meio poroso, ou quando temos um escoamento bifásico, ou uma outra situação similar é em geral inviável a tentativa de obtenção de campos de velocidade e tensão locais com a utilização de uma descrição local para cada um dos materiais em questão, como é feito em Mecânica do Contínuo Clássica.

A Teoria de Misturas surge então como uma ferramenta que procura viabilizar a solução de problemas, que não poderiam ser resolvidos com Mecânica do Contínuo Clássica, através de um ponto de vista diferente, onde se admite a superposição de contínuos dotados de cinemática independente. Este tipo de hipótese introduzirá novos termos nas equações de balanço de forma a manter uma coerência entre o fenômeno físico e a hipótese de superposição.

A primeira necessidade de uma nova definição aparece quando, admitindo que num mesmo ponto temos mais do que um contínuo, desejamos determinar a força exercida sobre uma certa superfície. Por exemplo seja um escoamento de água e ar num duto circular. Qual é a força exercida sobre a parede do duto? Classicamente, para efetuar este cálculo, precisaríamos conhecer os tensores tensão na água e no ar e aplicá-los às normais à superfície em questão, nos pontos onde existisse água ou ar respectivamente. Já considerando a água e o ar como uma mistura teremos que em cada ponto sobre a parede do duto haverá tanto a água quanto o ar. Assim, como a área banhada por cada um dos constituintes da mistura será toda a área da parede do duto, para que a força calculada seja a força real os tensores tensão considerados na água e no ar não podem ser os mesmos utilizados na Mecânica do Contínuo Clássica. Os tensores que serão considerados para a água e para o ar, neste caso, são chamados "Tensores Parciais de Tensão", sobre os quais voltaremos a falar.

Suponhamos agora que um fluido escoar em um meio poroso. É sabido que a matriz porosa altera o movimento do fluido uma vez que está em contato físico com este. Assim, uma vez que a Teoria de Misturas admite cinemática independente para os constituintes da mistura (sólido e fluido neste caso) é preciso que se leve em conta, na dinâmica, a interação entre os constituintes. Esta interação será dada pela chamada "Força Difusiva", que encontra sua mais clara e conhecida interpretação física na clássica experiência de Darcy que relaciona o gradiente de pressões com a velocidade de percolação em um meio poroso. Aqui a força de interação representa o arraste do fluido sobre a matriz porosa.

Neste trabalho estamos interessados em analisar o comportamento de um fluido Newtoniano que satura um certo meio poroso. Vamos procurar dar uma visão qualitativa e quantitativa para as grandezas que surgem naturalmente quando formulamos o problema à luz de Teoria de Misturas, utilizando para isto um paralelo com os conceitos clás

sicos de Mecânica do Contínuo. Este paralelo será baseado em situações físicas que podem ser tratadas tanto sob o ponto de vista de Teoria de Misturas quanto sob o ponto de vista de Mecânica do Contínuo Clássica.

EQUAÇÕES DE BALANÇO

Apresentaremos aqui, de forma sumária, as equações da continuidade e da quantidade de movimento para um contínuo simples e para cada constituinte de uma mistura.

Uma discussão detalhada pode ser encontrada em [1] para um meio contínuo e em [2] para misturas.

Equação da Continuidade e da Quantidade de Movimento para Um Meio Contínuo

Considerando ρ , \underline{v} , \underline{T} e \underline{g} como sendo respectivamente a densidade, o vetor velocidade, o tensor tensão e o vetor força de corpo por unidade de massa, definidos localmente para algum movimento de um material contínuo isotrópico, podemos escrever, para uma região R fixa no espaço (e ∂R sua fronteira)

$$\int_R \frac{\partial \rho}{\partial t} dV + \int_{\partial R} \rho \underline{v} \cdot \underline{n} dS = 0 \quad (1)$$

$$\int_R \rho \left(\frac{\partial \underline{v}}{\partial t} + (\text{grad} \underline{v}) \underline{v} \right) dV = \int_{\partial R} \underline{T} \cdot \underline{n} dS + \int_R \rho \underline{g} dV \quad (2)$$

ou, localmente

$$\frac{\partial \rho}{\partial t} + \text{div}(\rho \underline{v}) = 0 \quad (3)$$

$$\rho \left(\frac{\partial \underline{v}}{\partial t} + (\text{grad} \underline{v}) \underline{v} \right) = \text{div} \underline{T} + \rho \underline{g} \quad (4)$$

Aqui, o tensor tensão \underline{T} é simétrico para garantir o balanço de momento angular.

Equação da Continuidade e da Quantidade de Movimento para Cada Constituinte de uma Mistura Bifásica

Vejamos agora que equações devem ser obedecidas para misturas bifásicas (fluido+sólido, líquido+gás, etc.). Sejam então ρ_1 , \underline{v}_1 ,

\underline{T}_i , \underline{m}_i e \underline{g}_i respectivamente a densidade do constituinte i na mistura (massa do constituinte i /volume de mistura), sua velocidade, seu tensor parcial de tensões, a força difusiva exercida pelo outro constituinte e uma força de corpo por unidade de massa do constituinte i . Se agora tomarmos uma região fixa no espaço R teremos que, para cada constituinte

$$\int_R \frac{\partial \rho_i}{\partial t} d\mathbf{V} + \int_{\partial R} \rho_i \underline{v}_i \cdot \underline{n} dS = 0 \quad i = 1, 2 \quad (5)$$

$$\int_R \rho_i \frac{\partial \underline{v}_i}{\partial t} d\mathbf{V} + \int_R \rho_i (\text{grad} \underline{v}_i) \underline{v}_i d\mathbf{V} = \int_{\partial R} \underline{T}_i \underline{n} dS + \int_R \underline{m}_i d\mathbf{V} + \int_R \rho_i \underline{g}_i d\mathbf{V} \quad i = 1, 2 \quad (6)$$

onde estamos assumindo a não existência de reações químicas. Localmente podemos escrever que

$$\frac{\partial \rho_i}{\partial t} + \text{div}(\rho_i \underline{v}_i) = 0 \quad i = 1, 2 \quad (7)$$

$$\rho_i \left(\frac{\partial \underline{v}_i}{\partial t} + (\text{grad} \underline{v}_i) \underline{v}_i \right) = \text{div} \underline{T}_i + \underline{m}_i + \rho_i \underline{g}_i \quad i = 1, 2 \quad (8)$$

Suporemos que os tensores parciais de tensão são simétricos. Na equação (8) consideramos $\underline{m}_1 = \underline{m}$ e $\underline{m}_2 = -\underline{m}$, sendo \underline{m} a força exercida pelo constituinte 2 sobre 1. Uma vez que \underline{m}_1 e \underline{m}_2 são forças internas é necessário que sua soma seja nula em todos os pontos da mistura, por isto a definição acima.

MISTURA BIFÁSICA ESTÁTICA

Primeiramente vamos estudar uma situação estática envolvendo um arranjo formado por um cilindro que possui uma região preenchida por um fluido e por esferas sólidas formadas pelo mesmo material e do mesmo tamanho. Suporemos que não existe ação gravitacional e que a pressão nas seções A e B é a mesma.

Se assumirmos que forças intermoleculares são desprezíveis se comparadas com as forças clássicas de pressão podemos aplicar a equação (4) para um fluido estático à região entre as diversas esferas obtendo

$$\text{grad } p(x, y, z) = 0 \Rightarrow p = c^{te} \Rightarrow p_A = p_B = p \quad (9)$$

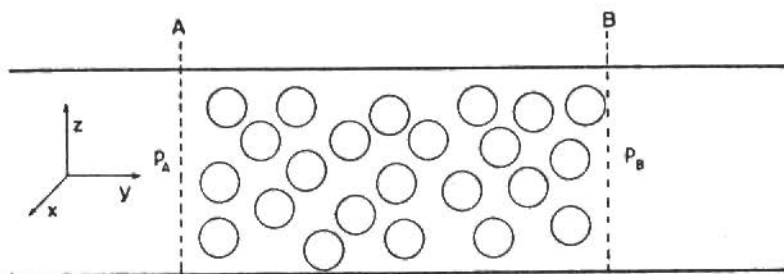


Figura 1. Cilindro cheio de fluido com esferas elásticas

Logo em cada ponto do fluido a pressão é a mesma e o tensor tensão no fluido é dado por

$$\underline{T}^* = -p \underline{1} \quad (10)$$

Isto faz com que cada uma das esferas esteja sujeita a um estado isotrópico de compressão radial (uma vez que estamos assumindo que as esferas não se tocam). Se pensarmos que as esferas são compostas por um material elástico homogêneo e isotrópico teremos que o tensor tensão em cada ponto de cada esfera será dado por

$$\underline{T}^{**} = \lambda (\text{tr } \underline{\epsilon}) \underline{1} + 2\mu \underline{\epsilon} \quad (11)$$

onde o tensor $\underline{\epsilon}$ é o tensor de deformação cujas componentes físicas são dadas em função do vetor deslocamento \underline{u} como (peq.def.)

$$\epsilon_{\langle rr \rangle} = \frac{\partial u_{\langle r \rangle}}{\partial r} \quad (12)$$

$$\epsilon_{\langle \theta \theta \rangle} = \frac{1}{r} \frac{\partial u_{\langle \theta \rangle}}{\partial \theta} + \frac{u_{\langle r \rangle}}{r} \quad (13)$$

$$\epsilon_{\langle \phi \phi \rangle} = \frac{1}{r \sin \theta} \frac{\partial u_{\langle \phi \rangle}}{\partial \phi} + \frac{u_{\langle r \rangle}}{r} + \frac{u_{\langle \theta \rangle} \cot \theta}{r} \quad (14)$$

$$\underline{\epsilon} = \epsilon_{\langle ij \rangle} \underline{e}_{\langle i \rangle} \otimes \underline{e}_{\langle j \rangle} \quad (15)$$

e, pela simetria das deformações $\epsilon_{\langle ij \rangle} = 0$ se $i \neq j$. Também pela

simetria teremos que

$$\epsilon_{\langle rr \rangle} = \frac{du_{\langle r \rangle}}{dr}, \quad \epsilon_{\langle \theta \theta \rangle} = \epsilon_{\langle \phi \phi \rangle} = \frac{u_{\langle r \rangle}}{r} \quad (16)$$

Uma vez que temos uma situação estática e sem forças de corpo temos que a equação (4) fica reduzida a

$$\text{div } \underline{T}^{**} = 0 \quad (17)$$

onde \underline{T}^{**} é o tensor tensão em cada esfera.

Uma vez que o tensor \underline{T}^{**} é função apenas da posição radial a equação (17) pode ser escrita como

$$\frac{1}{r^2} \frac{d}{dr} (r^2 T_{\langle rr \rangle}^{**}) - \frac{T_{\langle \theta \theta \rangle}^{**} + T_{\langle \phi \phi \rangle}^{**}}{r} = 0 \quad (18)$$

$$- \frac{\cotg \theta}{r} T_{\langle \phi \phi \rangle}^{**} + \frac{\cotg \theta}{r} T_{\langle \theta \theta \rangle}^{**} = 0 \quad (19)$$

o que leva a

$$\frac{2}{r} (T_{\langle rr \rangle}^{**} - T_{\langle \theta \theta \rangle}^{**}) + \frac{dT_{\langle rr \rangle}^{**}}{dr} = 0 \quad (20)$$

ou seja, substituindo (16) em (20)

$$2\mu \left(\frac{2}{r} \frac{du_{\langle r \rangle}}{dr} - \frac{2u_{\langle r \rangle}}{r^2} + \frac{d^2 u_{\langle r \rangle}}{dr^2} \right) + \lambda \frac{d}{dr} \left(\frac{1}{r^2} \frac{d}{dr} (r^2 u_{\langle r \rangle}) \right) = 0 \quad (21)$$

com as seguintes condições de contorno

$$\begin{aligned} u_{\langle r \rangle} &= 0 & \text{em} & \quad r = 0 \\ \frac{du_{\langle r \rangle}}{dr} &= p & \text{em} & \quad r = R \end{aligned} \quad (22)$$

A solução é $u_{\langle r \rangle} = cr$ o que nos leva a afirmar que

$$\text{ou} \quad T_{\langle rr \rangle}^{**} = T_{\langle \theta \theta \rangle}^{**} = T_{\langle \phi \phi \rangle}^{**} = -p \quad (23)$$

$$\underline{T}^{**} = -p \underline{1} \quad (24)$$

ou seja, os tensores tensão no fluido e no sólido são iguais.

Vamos agora transformar os resultados escrevendo-os sob o ponto de vista de teoria de misturas.

O problema aqui é o seguinte: Como escrever neste caso os tensores parciais de tensão no fluido e no sólido para assim determinar a pressão do fluido e do sólido na mistura e definir a pressão do poro?

Vejamos qual seria a força exercida sobre um plano imaginário que cortasse a região compreendida entre A e B.

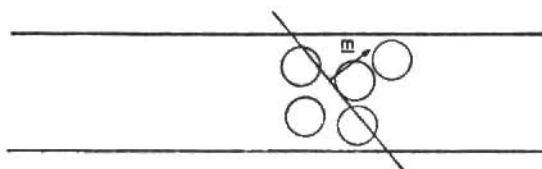


Figura 2. Plano imaginário cortando a mistura

$$\underline{F} = \int_{A_S} \underline{T}^{**} \underline{n} \, dS + \int_{A_F} \underline{T}^* \underline{n} \, dS \quad (25)$$

Se agora introduzimos o conceito contínuo de misturas podemos assumir que cada ponto entre A e B é ocupado simultaneamente por sólido e fluido. Assumindo uma distribuição uniforme das esferas temos que a fração em volume do fluido é igual à razão em área do mesmo, ou seja

$$\phi = \frac{\text{Volume do Fluido}}{\text{Volume da Mistura}} = \frac{\text{Área do Fluido}}{\text{Área da Mistura}} \quad (26)$$

Definamos os tensores parciais de tensão no sólido e no fluido como sendo os tensores que agindo num contínuo que ocupasse toda a mistura causariam o mesmo efeito causado pelo respectivo constituinte (sólido ou fluido). Denotando então por $\underline{T}_{\underline{f}}$ e $\underline{T}_{\underline{s}}$ os tensores parciais de tensão no fluido e no sólido respectivamente temos que

$$\int_{A_M} \underline{T}_{\underline{f}} \underline{n} \, dS = \int_{A_F} \underline{T}^* \underline{n} \, dS \quad (27)$$

$$\int_{A_M} \underline{T}_{\underline{s}} \underline{n} \, dS = \int_{A_S} \underline{T}^{**} \underline{n} \, dS \quad (28)$$

Podemos agora definir a pressão no fluido e no sólido como p_f e p_s , sendo dadas através da aplicação das equações (25), (26), (27) e (30) ao exemplo apresentado

$$\underline{F} = \int_{A_M} -p_s \underline{n} \, dS + \int_{A_M} -p_f \underline{n} \, dS \quad (29)$$

$$\underline{F} = \int_{A_F} -p \underline{n} \, dS + \int_{A_S} -p \underline{n} \, dS \quad (30)$$

onde A_F é a área real do plano onde existe o fluido, A_S é a área real do plano onde existe o sólido e A_M é a área total (ou área de mistura) que representa a soma das outras duas.

Sendo A_F , A_S e A_M como definidos acima, então

$$\phi A_M = A_F \quad (31)$$

$$(1 - \phi)A_M = A_S \quad (32)$$

Tomando (29), (30), (31) e (32) podemos escrever que

$$\underline{F} = \int_{A_M} p_s \underline{n} \, dS - \int_{A_M} p_f \underline{n} \, dS = - \int_{A_M} \phi p \underline{n} \, dS - \int_{A_M} (1 - \phi) p \underline{n} \, dS \quad (33)$$

Definimos então, por sugestão da equação (33)

$$p_s = (1 - \phi)p \quad (34)$$

$$p_f = \phi p$$

Neste caso:

p_s = pressão do sólido na mistura

p_f = pressão do fluido na mistura

p = pressão do poro

Os tensores parciais de tensão no fluido e no sólido são neste caso dados por

$$\underline{T}_f = -\phi p \underline{1} \quad (36)$$

$$T_s = -(1 - \phi) p \quad (37)$$

e deve ser notado que

$$P_f + P_s = P \quad (38)$$

MISTURA BIFÁSICA COM MOVIMENTO RELATIVO

Vamos estudar agora o escoamento de um fluido Newtoniano incompressível através de um meio poroso idealizado com o objetivo de dar uma visão qualitativa e quantitativa do que é a força difusiva neste caso.

Seja então um meio formado por um número infinito de placas paralelas infinitas, de mesma espessura, espaçadas de como mostra a figura. Entre estas placas faremos escoar, por efeito de um gradiente de pressões, um fluido Newtoniano incompressível com viscosidade constante. Entre cada duas placas teremos um escoamento de Couette.

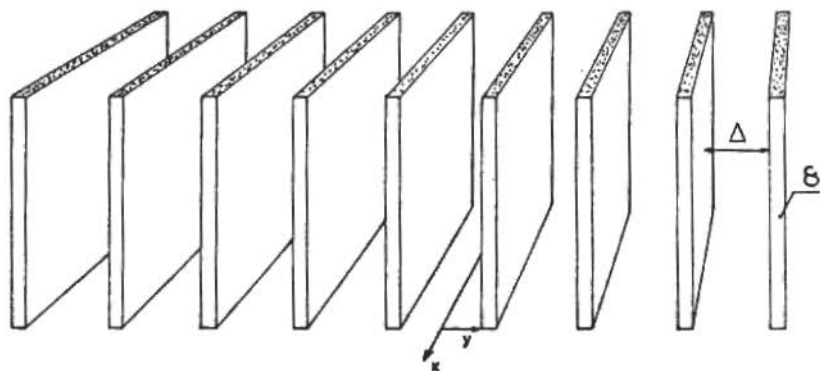


Figura 3. Meio poroso idealizado

Definindo $v_{<x>}$ como sendo a componente física do campo de velocidades na direção x para o fluido (sob o ponto de vista de mecânica dos fluidos clássica) obtemos de (4) que

$$v_{<x>} = \frac{-1}{2\eta} \frac{dP}{dx} \left[\left(\frac{\Delta}{2} \right)^2 - y^2 \right] \quad (39)$$

Para a obtenção de (39) foi assumido que a pressão só depende de x e que $v_{<x>}$ só depende de y , onde esta última variável é con

tada a partir do plano que equidista de cada duas placas na direção perpendicular a estas. Em (39) η é a viscosidade do fluido.

Vamos agora analisar o problema sob o ponto de vista de Teorema de Misturas.

Definindo a componente física do campo de velocidade do fluido na mistura como $v_{\langle x \rangle f}$ temos que

$$\int_{A_M} \phi v_{\langle x \rangle f} dS = \int_{A_F} v_{\langle x \rangle} dS \quad (40)$$

Façamos agora um paralelo com a experiência de Darcy. Esta experiência mostra que um fluido Newtoniano escoando por um meio poroso homogêneo por efeito de um gradiente de pressões obedece a

$$v = - \frac{K}{\eta} \left[\frac{dP}{dx} \right] \quad (41)$$

onde K é a permeabilidade da matriz porosa e η sua porosidade. A velocidade v é chamada de velocidade de percolação, sendo calculada como a razão entre a vazão real de fluido e a área total (área de escoamento + área de sólidos).

Considerando agora o meio poroso ideal com o qual estamos trabalhando podemos calcular analiticamente sua porosidade e sua permeabilidade, sendo a primeira dada por

$$\phi = \frac{\Delta}{\Delta + \delta} \quad (42)$$

Se combinarmos a equação (41) com a média da equação (39), levando em conta que esta última deve ser tomada sobre a área total de mistura, temos que

$$\bar{v}_{\langle x \rangle} = \frac{-1}{3\eta} \frac{dP}{dx} \left(\frac{\Delta}{2} \right)^2 \quad (43)$$

$$v = \phi \bar{v}_{\langle x \rangle} \quad (44)$$

$$\frac{K}{\phi} = \frac{\Delta^2}{12} \quad (45)$$

o que nos permite escrever que

$$K = \frac{\Delta^3}{12(\Delta + \delta)} \quad (46)$$

Uma vez que sob o ponto de vista de Teoria de Mistura não existem, para o escoamento estudado, variações na direção (perpendicular às placas) então

$$v_{\langle x \rangle f} = \bar{v}_{\langle x \rangle} = \text{constante} \quad (47)$$

o que nos permite escrever, com o auxílio de (41), (43) e (44)

$$\phi v_{\langle x \rangle f} = \phi \bar{v}_{\langle x \rangle} = \frac{-\phi}{3\eta} \frac{dP}{dx} \left(\frac{\Delta}{2} \right)^2 = - \frac{K}{\eta} \frac{dP}{dx} \quad (48)$$

A força de interação sólido-fluido neste caso é a força que o sólido exerce sobre o fluido através do cisalhamento nas paredes. Esta força é dada por

$$\underline{F}_t = -2 \int_A \tau \underline{e}_{\langle y \rangle} dS \quad (49)$$

$$\underline{F}_t = -2 \left. \frac{dv_{\langle x \rangle}}{dy} \right|_{y=-\frac{\Delta}{2}} A \underline{e}_{\langle x \rangle} = \Delta \frac{dP}{dx} A \underline{e}_{\langle x \rangle} \quad (50)$$

onde A é a área lateral de cada placa considerada. Como o escoamento se processa na direção x a força cisalhante atua na mesma direção.

Sob o ponto de vista de misturas esta força é dada pela integral do vetor \underline{m} (que aparece em (8) representando a força de interação, ou difusiva, que o sólido exerce sobre o fluido) sobre um volume de mistura correspondente à área A considerada em (49) e (50). Assim

$$\underline{F}_t = \int_{V_M} \underline{m} dV \quad (51)$$

Uma vez que para o caso considerado a força de interação, ou difusiva, é a mesma em todos os pontos da mistura, temos

$$\underline{F}_t = \underline{m} V_M = \Delta \frac{dP}{dx} A \underline{e}_{\langle x \rangle} \quad (52)$$

onde

$$V_M = (\Delta + \delta) A \quad (53)$$

o que implica em

$$\underline{m} = \frac{\Delta}{\Delta + \delta} \frac{dP}{dx} \underline{e}_{\langle x \rangle} = \phi \frac{dP}{dx} \underline{e}_{\langle x \rangle} \quad (54)$$

Combinando (54) com (48) chegamos a

$$m_{\langle x \rangle} = - \frac{\phi^2 \eta}{K} v_{\langle x \rangle} f \quad (55)$$

onde $m_{\langle x \rangle}$ é a componente física do vetor \underline{m} na direção x .

Conseguimos então uma expressão para a força difusiva em função da velocidade do fluido na mistura que poderia ser extrapolada para

$$\underline{m} = - \frac{\phi^2 \eta}{K} \underline{v}_f \quad (56)$$

A equação (54) combinada com (8), dentro das hipóteses do problema, levaria a

$$(\text{div } \underline{T}_f) \cdot \underline{e}_{\langle x \rangle} = - \phi \frac{dP}{dx} \quad (57)$$

ou seja

$$\underline{T}_{\langle xx \rangle} = - \phi p = - p_f \quad (58)$$

onde novamente aqui p_f é a pressão do fluido na mistura.

Se assumirmos que as componentes físicas do tensor parcial de tensão no fluido $T_{\langle xy \rangle}$, $T_{\langle yz \rangle}$ e $T_{\langle xz \rangle}$ dependem linearmente do gradiente de velocidade do fluido na mistura podemos dizer que, neste caso

$$\underline{T}_f = - p_f \underline{1} = - \phi p \underline{1} \quad (59)$$

O que foi desenvolvido aqui dá uma motivação para se empregar a clássica relação $\underline{m} \propto \underline{v}_f$ em escoamentos em meios porosos e para termos definido p_f como na seção anterior.

COMENTÁRIOS FINAIS

Neste trabalho apresentou-se uma interpretação física para o tensor parcial de tensão e para a força de interação sólido-fluido, assim como uma motivação para seus empregos em certos casos.

A discussão aqui ficou restrita a misturas binárias sólido-fluido e a casos bem particulares. São estes casos simples, porém, que nos permitem visualizar entidades como \underline{T}_i e \underline{m}_i , as quais diferem muito daquelas comumente usadas nas teorias clássicas.

São situações simples, como as aqui discutidas, que nos permitem estender os conceitos associados à teoria contínua de misturas, possibilitando a descrição de fenômenos mais complexos sob este ponto de vista.

REFERÊNCIAS

- [1] Billington, E.W. and Tate, A. - The physics of deformation and flow. McGraw-Hill (1981).
- [2] Atkin, R.J. and Craine, R.E. - Continuum theory of mixtures: Basic theory and historical development. Quart. J. Mech. Appl. Math., XXIX (2), 1976.

STABILITY ANALYSIS OF DISSIPATIVE NONLINEAR DYNAMICAL SYSTEMS

Edwin J. Kreuzer

Institute B of Mechanics

University of Stuttgart

Pfaffenwaldring 9

D-7000 Stuttgart 80, F.R.G.

ABSTRACT

Much recent progress in the study of stability of nonlinear dynamical systems is related to the use of computers. Fortunately most technical dynamical systems are dissipative. In general, in a dissipative system, the set of all orbits converge as time passes to a compact set of the phase space, a so-called attractor, and remain there. Thus, the relevant objects in the stability analysis of dissipative systems are attractors. Using Lyapunov exponents, the dimension of attractors, the cell mapping approach, and the entropy concept we are in a position to analyze numerically the longtime behavior of nonlinear dynamical systems.

INTRODUCTION

Many new problems in nonlinear dynamics have emerged in the analysis and design of even simple dynamical systems. Since for most technical devices and control systems the relevant factors are naturally described by nonlinear mathematical models, there is a growing interest in the analysis of nonlinear dynamics in applied dynamics. Nonlinear dynamics are in many ways quite different from linear dynamics.

One advantage of technical systems is that they are usually dissipative. For such systems exist subsets of the phase space

which attract neighboring points. These subsets are called attracting sets or attractors. If we do not care about the transient behavior of orbits, but only about the behavior that will persist eventually, then knowledge of attractors is of major concern. Hence, the typical behavior of dissipative systems is described in terms of a system. What happens near an attractor or sink is of special interest in applications. On the other hand, in engineering we can find many problems where different kinds of attractors coexist in a domain of interest of the phase space. Hence, we would like to know the set of initial states from which a certain attractor is attainable. This set of initial states forms the basin of attraction of an attractor.

Simplest of all is the steady-state case (fixed point of the dynamical systems), then the oscillation (or periodic behavior); but recent studies have shown how easy it is to have far more complicated attractors appear. In particular, even the structurally stable attractors in rather simple examples contain a vast mixture of periodic, quasiperiodic, homoclinic, and other kinds of phenomena. These varieties of behavior and related attractors occur due to parameter changes, that is: as a parameter slowly changes, the motion may change from regular to chaotic and vice versa. Analytical solutions for such motions are rarely available. Modern computer technology allows us to simulate systems more or less easily and together with geometrical considerations we may gain essential insights.

But to locate an attractor of a nonlinear dynamical system and to determine its basin of attraction may be quite time consuming. This is particularly true if small differences in the initial conditions produce very great ones in the final behavior. Then, conventional methods or even choosing many initial states at random may be unsatisfactory. The complexity of nonlinear dynamical systems suggests, especially for systems exhibiting chaotic motions, that a statistical description may be of more use than the actual knowledge of the time evolution.

In view of the above considerations, it seems desirable to give a precise mathematical definition of attractors. One would like the definition to satisfy various requirements, and it turns out in the following section, that the requirements may be somewhat

conflicting. In the subsequent section we shall classify dynamical systems by means of attractors commonly found in mechanics and describe different features characterizing them. Following we shall introduce the cell mapping theory for analysis of nonlinear dynamical systems. Thereupon, the relationship of cell mappings to Poincare maps is described and some mathematical details are given. Using the cell mapping approach the location of attractors and their domains of attraction are found in a very efficient manner. Next section we shall introduce the concept of entropy and argue that, under suitable conditions, this concept allows the prediction of the asymptotic behavior depending on initial conditions. We shall then treat an example and in the last section conclude with some further remarks.

A DEFINITION OF ATTRACTORS

The evolution of a system, for fixed value of the parameter, will be described by N first-order differential equations of the form

$$\dot{\mathbf{x}} = \mathbf{f}(\mathbf{x}) \quad , \quad (1)$$

where \mathbf{x} and \mathbf{f} are vectors in \mathbb{R}^N and \mathbf{f} is explicitly independent of time. Hence, the phase space for this system is N -dimensional, with coordinates x_i , $i = 1, \dots, N$. Autonomous systems often have an even dimension N . A non-autonomous mechanical system can be written in form (1) by extending the number of coordinates by one; the dimension is therefore no longer even.

When dealing with a dissipative dynamical system we may start in a Euclidean phase space of initial conditions of large dimension N ; after some time passes, the transients relax, some modes may damp out, and the state of the system approaches a lower dimensional subspace of the \mathbb{R}^N with a volume contracting rate defined as

$$\sum_{i=1}^N \frac{\partial f_i}{\partial x_i}(\mathbf{x}) < 0 \quad . \quad (2)$$

The number of degrees of freedom is thereby reduced. We call the subspace of the \mathbb{R}^N to which the solution of the dynamical system asymptotes for large time an attractor. An elaborate

description of requirements an attractor must satisfy, with definitions and proofs, is given in Ruelle [1]. There is, however, no overall accepted definition of attractors; we rely on Eckmann [2].

Definition: An attractor for the flow of (1) is a compact set A satisfying

- (i) A is invariant under the flow.
- (ii) A has a shrinking neighborhood, i.e., there is an open neighborhood around A that shrinks down to A under the flow.
- (iii) The flow on A is recurrent, i.e., no part of A is transient.
- (iv) A cannot be decomposed into two nontrivial closed invariant pieces.

If A is an attractor, its basin of attraction is defined to be the set of all initial points x such that the flow approaches A as $t \rightarrow \infty$.

For one-dimensional flows, the only possible attractors are stable fixed points or sinks. For a two-dimensional flow within a finite section of a plane, the Poincare-Bendixson Theorem shows that the only possible attractors are fixed points or sinks, and periodic solutions (simple closed curves) or limit cycles. In three-dimensional phase space where $\sum_i \frac{\partial f_i}{\partial x_i}$ is not everywhere negative or in more than three-dimensional phase space torus attractors are possible.

Remarks: Of course, there may be systems where a torus can be attractive but where it is not an attractor. E.g., a doubly periodic motion on a torus, defined by a rational winding number, does not fulfill property (iv) and is thus not a torus attractor but rather a complicated periodic cycle. On the other hand if the winding number is irrational, the motion on the attractor may be quasiperiodic and a trajectory will eventually cover the torus completely, then we speak of a torus attractor. Consequently, when we say a set is an attractor, we do not only mean that it is attractive, but also that it is transitive: that is, most trajectories on it wander all over it.

Torus attractors of more than two dimensions are extremely rare and will therefore not be considered here. They give way to attractors with unpredictable or chaotic behavior which are neither fixed points nor periodic orbits, so-called strange attractors. These are asymptotic limit sets in phase space which also have lower dimension than the phase space and which have an additional property: the motion on the attractor is characterized by an exponential divergence of neighboring states in some direction. This effects a sensitive dependence on initial conditions and is the cause for their strange appearance. It also practically prevents long-term predictions since the initial conditions are usually not known exactly. Similarly, for a chaotic system, the information one can gain about its state from information about an initial state decays (until zero) roughly linearly in time.

It is important to note that the irregular behavior is self-generated by a purely deterministic system. It is even more important to emphasize, that systems of deterministic differential equations exhibiting chaotic behavior are a striking contrast to random motions produced by Gaussian noise. Chaotic systems provide a very different notion of randomness. For a thorough description of this difference, especially the peaceful coexistence between chaos and order, see Farmer [3].

Deterministic systems can generate a variety of different types of irregularity, with a variety of manifestations of internal order. Thus, neither an external noise, nor complexity is required to produce chaos. Procedures which are able to distinguish between chaos and randomness are suggested by Guckenheimer [4]. These procedures are based on the assumption that randomness means unpredictability in the short-term evolution of a system. Chaos, however, is characterized by an exponential divergence of neighboring states in phase space which prevents long-term prediction.

CLASSIFICATION OF DISSIPATIVE DYNAMICAL SYSTEMS

The initial hope in the study of dynamical systems was to classify dynamical equations up to equivalence in some qualitative sense, Smale [5]. Although this goal can be achieved for certain restricted classes of systems, an appropriate and useful equivalence relation has not been found for which it can be achieved in general.

One would like to classify dynamical systems so as to include qualitative features of their behavior, though which features one should consider is not a priori known and may even depend on the specific problem. Most interest is focussed on longtime behavior of orbits, in dissipative systems characterized by attractors. However, a physical system might not reach its attractor on a practical time scale, hence, a classification of dynamical systems should also cover transient motions. Although we are far from a complete classification of dynamical systems, we will describe at least four basic features of an attractor.

Time history is a common way to classify a system. The single trajectories may be either regular or irregular and unpredictable. Furthermore, when an irregular time series is observed in an experiment one may ask whether the irregularity is due to chaos or to randomness as distinguished above. When little is known about the system, one can only hope that the time series possesses intrinsic properties which make this distinction possible. It may often be difficult to detect periodicity, bifurcations, etc.

Power spectra of time histories indicate regular or chaotic motion. A discrete power spectrum, i.e., one that consists of discrete vertical line segments, is characteristic for periodic and quasiperiodic attractors. A continuous or noisy power spectrum implies the existence of a strange attractor. Since the power spectrum is easily studied experimentally, the prediction about systems behavior can be tested by physical experiments. But in general, power spectra analysis is of little help in distinguishing between chaotic behavior and irregular behavior produced by external noise.

Lyapunov exponents measure how fast nearby orbits diverge or converge. Or in other words, the Lyapunov exponents are an average of the local stability properties of an attractor. For a fixed point, for example, the Lyapunov exponents are the real parts of the eigenvalues. The Lyapunov exponents are generalized stability exponents, defined for any type of attractor. For an N -dimensional phase space, there are N real exponents that can be ordered as

$\lambda_1 \geq \lambda_2 \geq \dots \geq \lambda_N$ and one of the exponents representing the direction along the flow, being zero. If $\lambda_1 > 0$ then the system is chaotic. Hence, the sensitive dependence and the degree of unpredictability are measured by a positive Lyapunov exponent. For dissipative systems the spectrum of Lyapunov exponents describes not only the stability behavior of single orbits but characterizes the dynamics of the whole domain of attraction. Lyapunov exponents can only be determined if the system's equations are available.

Dimension is perhaps the most basic property of an attractor. We may think of the dimension as giving, in some way, the amount of information necessary to specify the position of a point on the attractor to within a given accuracy. Then, dimension says something about the amount of information necessary to characterize the attractor. The dimension is also a lower bound on the number of essential variable needed to model the dynamics. We define dimension in terms of Lyapunov exponents because they provide the only known efficient method to compute dimension:

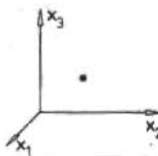
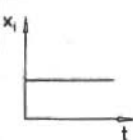
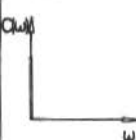
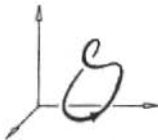

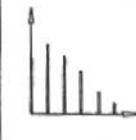
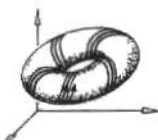
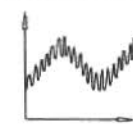
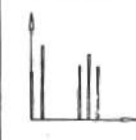

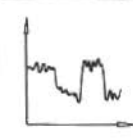
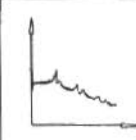
$$D_L = k + \frac{\sum_{i=1}^k \lambda_i}{|\lambda_{k+1}|} \quad (3)$$

where k is the largest integer so that $\lambda_1 + \lambda_2 + \dots + \lambda_k \geq 0$. This definition was introduced by Kaplan and Yorke [6] and is called Lyapunov dimension.

In the literature other different definitions of dimension may be found. For simple, predictable attractors such as fixed points, limit cycles, or 2-tori, the separate notions of dimension converge; by any reasonable definition these attractors are of dimension 0, 1 or 2, respectively. It is because their structure is very regular that the dimension of these attractors take on integer values. Strange attractors, however, often have a structure that is not simple; they are often not manifolds, and frequently have a highly fractured character. Hence for a strange attractor D_L is noninteger so that the volume of the attractor is zero. Consequently, attractors of zero volume need not only dimension zero, one or two, but can in fact have a noninteger dimension.

Table 1 gives a summary of the attractors presented, with sketches of their characteristic output, their Lyapunov exponents, and their dimension.

Table 1. Attractors and their basic properties

Phase Portrait	Time History	Power Spectrum	Lyapunov Exp. $\lambda_1 \geq \lambda_2 \geq \lambda_3$	Dimension
			- - -	0
			0 - -	1
			0 0 -	2
			+ 0 -	$2 < d < 3$

STABILITY ANALYSIS USING THE CELL MAPPING APPROACH

Basic questions in the stability analysis of dissipative dynamical systems are: where is an attractor located in the phase space, what does the attractor look like, what is its basin of attraction. We are often obliged to answer these questions with the aid of a computer. The engineering systems, however, have become very complex and variation of parameters may often change behavior so essentially that trial and error may often fail. The difficulties can sometimes be overcome by sophisticated analytic methods. Furthermore, not only the form of an attractor can be complicated, but also its basin of attraction, even if the attractor is simple. Hence, there is a need for a method to solve at least some of the problems mentioned. Hsu [7,8] proposed the cell mapping theory as a mean for analysis of nonlinear dynamical systems.

Computer programs are described by Hsu and Guttalu [9] and Hsu, Guttalu, and Zhu [10]. Modifications and extensions of a cell mapping algorithm may be found in Bestle and Kreuzer [11] and a thorough description is given in [12]. The method is still under development, but has already proved its applicability in many problems. A cell mapping is essentially a discretization of a Poincaré mapping.

It is often helpful to treat time as if it were discrete. This is particularly true for autonomous systems or for systems affected by conditions varying periodically with time. The continuous system (1) is consequently replaced by difference equations designed to model the Poincaré map of (1). An orbit is replaced by a set of points obtained by repeated application of the mapping. Such a mapping can be explored more quickly and extensively than the continuous system, since the essential properties of the orbits are preserved as corresponding properties of the set of points. Sometimes we can guess at an appropriate mapping or find analytic approximations; however, usually only numerical integration methods will provide us with a Poincaré map. The definition of a Poincaré map is based on a so-called surface of section Σ . For a non-autonomous mechanical system of one degree of freedom, the construction is rather obvious, if the system is forced by an input with a certain period. Then, we normally plot the intersection of an orbit with the phase plane at the instants of time given by the period of the input. In this way we construct the map

$$\mathbf{y}(n+1) = \mathbf{g}(\mathbf{y}(n)) \quad , \quad \mathbf{g}: \mathbb{R}^{N-1} \rightarrow \mathbb{R}^{N-1} \quad (4)$$

where \mathbf{y} and \mathbf{g} are vectors in \mathbb{R}^{N-1} and one should think of n as the discrete time. If f of (1) is smooth and the surface $\Sigma := \mathbb{R}^{N-1}$ is everywhere transverse to f , then it can be shown that the Poincaré map \mathbf{g} is also smooth.

Although the determination of basins of attraction by means of a Poincaré mapping is greatly improved, the method also has its drawbacks. Numbers in a computer are represented only within a finite accuracy. Hence, it is not possible to consider a Poincaré map as a continuum of points. It turns out that for practical purposes approximating a Poincaré map by a collection of very small cells describes the dynamical system sufficiently well.

After choosing a domain of interest $\Omega \subset \Sigma$ we partition this domain in N_r subdomains $\Omega_i \subset \Omega$. The Ω_i 's are the so-called regular cells numbered 1 to N_r . The region $\Omega_0 = \Sigma/\Omega$ forms one single cell, the so-called sink cell or 0th cell. Regular cells and the sink cell form the cell space $S = \{0, 1, \dots, N_r\}$. Setting up a cell space in this manner we replace the continuous Poincaré map by a discrete cell map. Consequently, this leads to a new discrete state or random variable ξ defined by

$$\xi(n) = i \in S \quad \longleftrightarrow \quad \mathbf{y}(n) \in \Omega_i . \quad (5)$$

Hence, the state of the system at time n is no longer described by a point $\mathbf{y}(n)$ in Σ but by the probability $\zeta_i(n)$ of which the point $\mathbf{y}(n)$ is found in cell Ω_i at time n :

$$\zeta_i(n) = \text{Pr}[\xi(n) = i] \quad , \quad i \in S . \quad (6)$$

Summarizing all probabilities $\zeta_i(n)$ by a cell probability vector $\zeta(n)$, the evolution of the system is described by a finite, discrete, stationary Markov chain defined as

$$\zeta(n+1) = \mathbf{P} \zeta(n) \quad , \quad n = 0, 1, 2, \dots , \quad (7)$$

where \mathbf{P} is the matrix of transition probabilities with components

$$p_{ij} = \text{Pr}[\xi(n+1) = i \mid \xi(n) = j] \quad , \quad i, j \in S . \quad (8)$$

The p_{ij} 's define the one-step transition probabilities for the system moving from cell j to cell i . Together with an initial probability distribution the transition probability matrix \mathbf{P} completely describes the evolution process of a dynamical system.

The long term behavior of a Markov chain is classified by means of a partitioning of the cell space S into a closed subset of cells forming persistent groups and an open subset of cells forming the transient group. A persistent group cannot be further decomposed. Hence, it is obvious that attractors of dynamical systems are represented by persistent groups for which a period and a limiting probability distribution can be defined.

If the system starts in the group of transient cells it will leave them with the probability one. It will be absorbed in different persistent groups with certain absorption probabilities and within certain expected absorption times. Hence, transient cells form the basins of attraction.

ENTROPY AND SHORT-TERM PREDICTIONS

The entropy concept is related to familiar properties of a dynamical system and is a natural way to study statistical properties: probability leads to entropy, or in other terms, to information, e.g., Farmer [13]. We will review these matters below.

The amount of information gained in making an observation of a physical system depends on the a priori knowledge of the observer making the measurement. Our knowledge is the equations of motion and all information that can be extracted from them. A measurement can never be made with infinite precision, i.e., in practice, positions are given approximately to within ϵ . Thus, at best a highly localized probability distribution can be prescribed. Therefore, prediction must be discussed in terms of ensembles of initial conditions rather than in terms of the behavior of individual points.

A natural way to do this is to partition the attractor by dividing it into many discrete cells as was described in section 4. For an attractor A, let $M(\epsilon)$ be the minimum number of cells that can be chosen so that the cubes of size ϵ cover the attractor. If $P_i(\epsilon)$, $i = 1, \dots, M(\epsilon)$, describes the probability contained within the i th cube we have

$$\sum_{i=1}^{M(\epsilon)} P_i(\epsilon) = 1 \quad (9)$$

The amount of information necessary to specify the state of the system to within an accuracy ϵ is defined as

$$I(\epsilon) = - \sum_{i=1}^{M(\epsilon)} P_i(\epsilon) \ln P_i(\epsilon) \quad (10)$$

It is also the information obtained in making a measurement that is uncertain by an amount ϵ .

Using this definition, the information dimension is given by

$$D_I = \lim_{\epsilon \geq 0} \frac{I(\epsilon)}{\ln(1/\epsilon)} \quad (11)$$

It tells us how the information grows as ϵ shrinks to zero. Since for small ϵ

$$I(\epsilon) \approx D_I \ln(1/\epsilon) \quad (12)$$

we may view D_I as telling how fast the information necessary to specify a point on the attractor increases as ϵ decreases.

So far we have been concerned with the amount of information gained by an observer in making a single, isolated measurement. But how much new information is gained about an initial condition with successive extra measurements. For a predictable system new measurements provide no further information. For a chaotic system, however, on the average trajectories diverge locally at an exponential rate, and each successive measurement provides new information. The Kolomogorov-Sinai entropy (KS entropy) provides an upper bound on the information acquisition rate; Lichtenberg, Lieberman [14].

The KS entropy is defined by using a partition of phase space as described above. By definition, the KS entropy is positive for a chaotic attractor, i.e., when there is an exponential decrease in the average measure of an element of the partition. Hence, it is not surprising to learn, that the KS entropy is related to the average rate of exponential divergence of nearby orbits, i.e., to the Lyapunov exponents. The following relation was found by Pesin [15] for Lyapunov exponents depending on initial conditions:

$$h_\mu = \int_B \left\{ \sum_{\lambda_i(\mathbf{x}) > 0} \lambda_i(\mathbf{x}) \right\} p(\mathbf{x}) d\mathbf{x} \quad (13)$$

where h_μ is the metric entropy, $p(\mathbf{x})$ is the probability density, the sum is that of all positive Lyapunov exponents and the integral is for a specified region of phase space. The KS entropy is generally understood to be a measure applied to a single region of chaotic behavior, excluding regular regions, embedded islands etc. In this case the λ 's are independent of \mathbf{x} and (13) results in

$$h_{\mu} = \sum_{\lambda_i > 0} \lambda_i \quad . \quad (14)$$

The information $I(t)$ decreases initially at a linear rate, Figure 1. Thus, at a given level of precision the metric entropy and information dimension can be used to estimate $I(t)$ for short times. Let the information associated with the initial distribution of points be $I(0) = D_I \ln 1/\epsilon$. Then the time-dependence of the information is given by

$$I(t) = I(0) - h_{\mu} t = D_I \ln \frac{1}{\epsilon} - h_{\mu} t \quad . \quad (15)$$

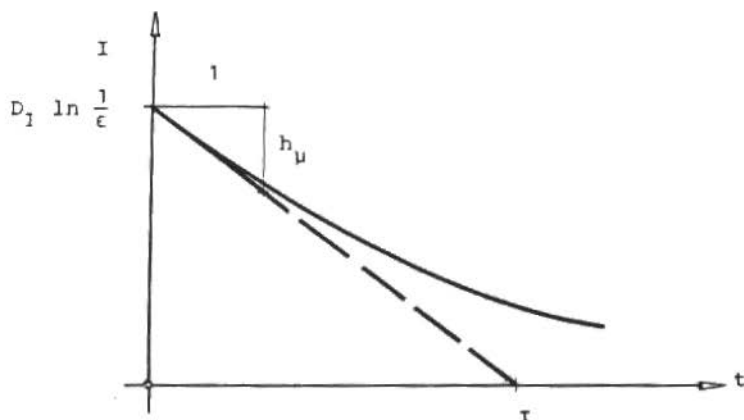


Figure 1. Typical behavior of $I(t)$ for a chaotic attractor

Thus, information about initial state is lost after a characteristic time

$$\tau = \frac{D_I \ln 1/\epsilon}{h_{\mu}} \quad . \quad (16)$$

It is clear that increasing the accuracy of a measurement increases the information obtainable. Consequently, as we increase our resolution, we increase the information, and we could think of an arbitrary high value if we decrease the cell size to zero. But, as has already been discussed in section 4, reality limits the information we can obtain from a system to a certain degree.

Kaplan and Yorke [6] conjecture that for all but exceptional cases $D_L = D_I$ (area conserving flows are an exceptional case). The Lyapunov exponents and hence the Lyapunov dimension are much easier to compute than the information dimension. Thus, with the Lyapunov exponent at hand we have also an efficient tool to study information decay.

EXAMPLE

A nonlinear oscillator with a cubic stiffness term to model the progressive spring effect observed in many mechanical systems is described by Duffing's equation. We will use a modification of the conventional Duffing equation in which the linear stiffness term is neglected. Hence we use the Duffing equation in the form

$$\ddot{x} + a\dot{x} + x^3 = b \cos t, \quad (17)$$

where x , \dot{x} represent the displacement and velocity, the dissipation is modeled by a linear velocity dependent term with parameter a , and the forcing term on the right hand side is characterized by an amplitude b . Such an equation was studied at some length by Ueda [16], using analog and digital computers, for the parameters $a \in (0., 0.8)$ and $b \in (0., 25.)$.

For low force amplitudes b we observe periodic motions. As b is slowly increased, a point comes at which the system suddenly begins to jump back and forth in an irregular, chaotic manner. These phenomena are summarized in Figure 2. Chaotic motions take place in the shaded regions. In the area hatched by full lines, chaotic motion occurs uniquely, while in the area hatched by broken lines, two different types are observed, i.e., chaotic and regular motions. Which one occurs depends on the initial conditions.

Without performing a detailed analysis of all phenomena occurring in this simple example we will calculate Lyapunov exponents only for parameter values where $b = 7.5$ and $a \in (0.04, 0.25)$. These parameters are indicated in Figure 2 by the heavy line.

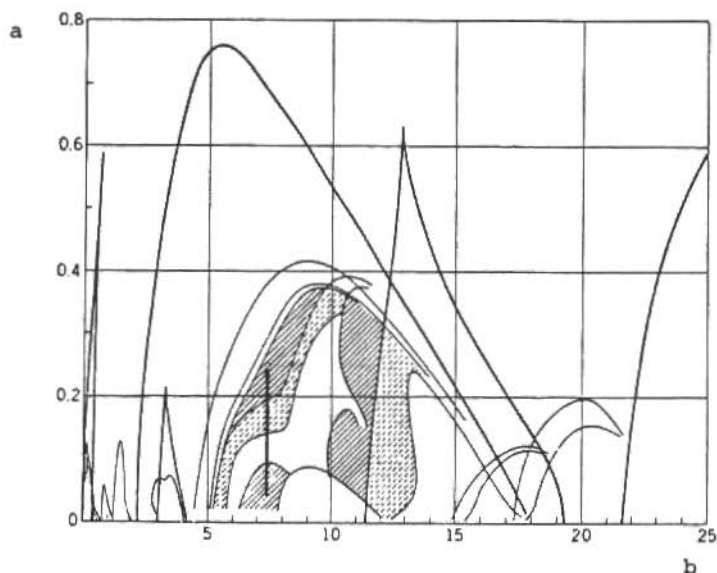


Figure 2. Regions of different dynamical properties of (17) in the parameter plane, from Ueda [16]

For numerical simulations (17) is rewritten as an autonomous system of three first order equations letting $y_1 = x$, $y_2 = \dot{x}$, and $y_3 = t$

$$\left. \begin{aligned} \dot{y}_1 &= y_2 \quad , \\ \dot{y}_2 &= -y_1^3 - ay_2 + b \cos y_3 \quad , \\ \dot{y}_3 &= 1 \quad , \end{aligned} \right\} (y_1, y_2, y_3) \in \mathbb{R}^2 \times S^1 \quad . \quad (18)$$

Here, $S^1 = \mathbb{R}/T$ is the circle of length $T = 2\pi$. The surface of section we define as $\Sigma = \{(y_1, y_2, y_3) \mid y_3 = 0\}$. The Poincaré map $P: \Sigma \rightarrow \Sigma$ is globally defined. Clearly, P depends upon the parameters a and b .

We first describe the results of the computed Lyapunov exponents. In Figure 3 is shown the spectrum of Lyapunov exponents. The results presented here are taken from Kleczka [17]. The following phenomena are observed:

- Chaotic behavior: $a \in (0.04, 0.09) \cup (0.15, 0.22) \cup (0.23, 0.25)$

- Regular windows: $a \in (0.09, 0.19)$, $(0.22, 0.23)$
- Bifurcations: at $a \approx 0.115, 0.096, 0.0925$
- Coexistence of chaotic and regular behavior:
 $a \in (0.15, 0.19)$

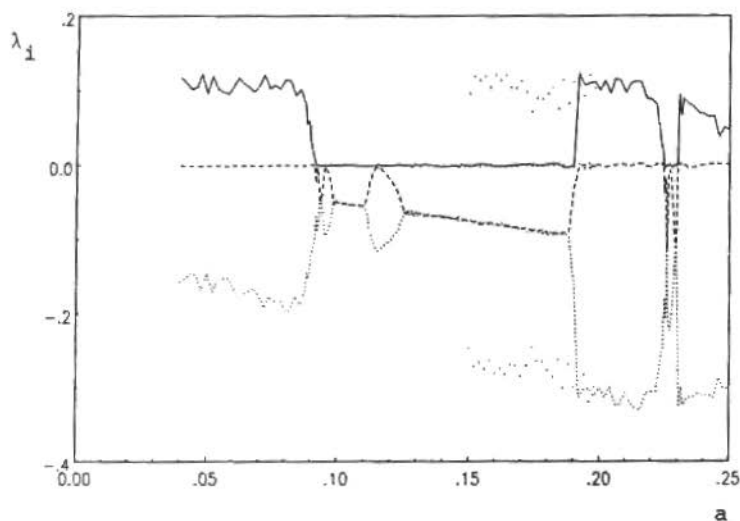


Figure 3. Spectrum of Lyapunov exponents depending on a

Of course, the Poincaré map for this example can only be found numerically. From that the cell mapping is automatically constructed by means of a computer program, e.g., [12]. As mentioned above, system (18) shows regular behavior with harmonic and subharmonic solutions for a wide range of parameters. For some parameters, however, the system exhibits chaotic behavior and for others both periodic and chaotic behavior. For such parameter values, here $a = 0.1$ and $b = 12.0$, where chaotic and periodic solutions coexist, we show the cell mapping results.

Figure 4 and 5 show the results obtained for (18) by using the generalized cell mapping procedure. In both figures the number of intervals in each direction is $N_{C1} = N_{C2} = 100$ covering $-1.5 \leq y_1 < 4.5$ and $-10.0 \leq y_2 < 8.0$.




The expected absorption probability of transient cells into the cells of the two persistent groups denoted by  is shown in

Figure 4. The small persistent group replaces the strange attractor. The absorption probability is 100% for transient cells shown; cells signified by  are absorbed into the periodic solution and cells signified by  are absorbed by the chaotic attractor.

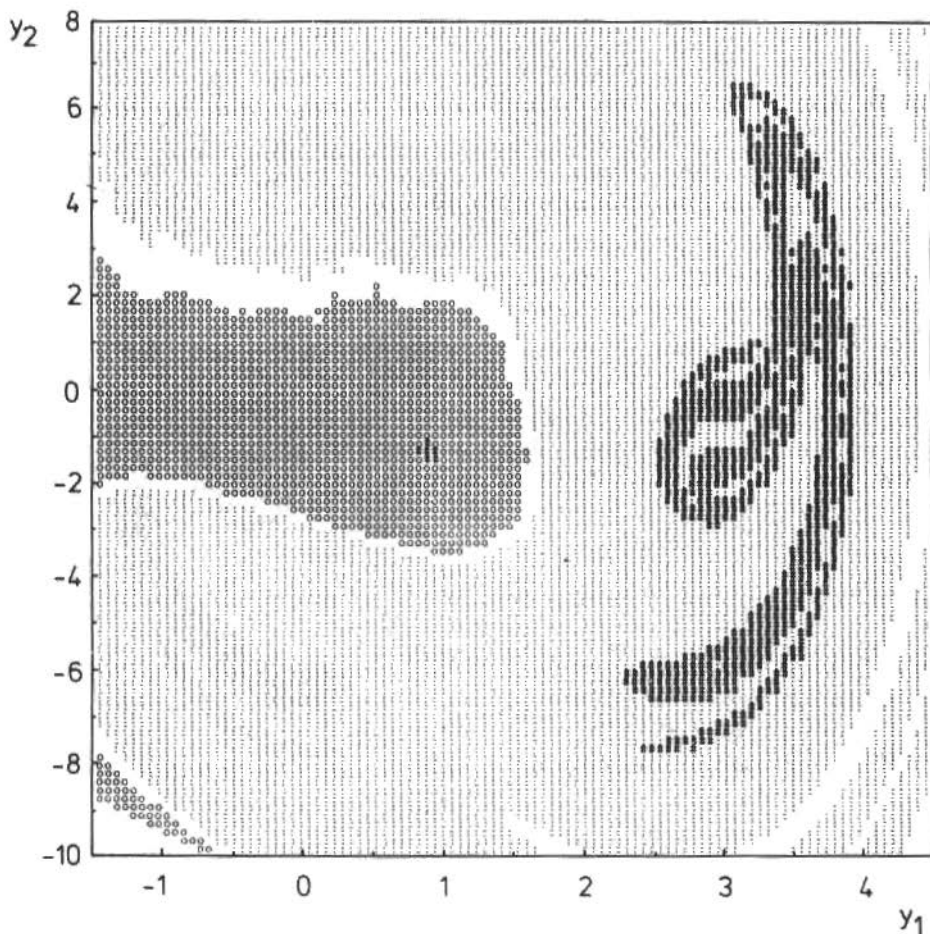


Figure 4. Absorption probability of transient cells into persistent groups

The expected absorption time of transient cells being absorbed into cells \blacksquare of the persistent groups is illustrated by Figure 5. For both groups the cells are indicated again by different symbols to characterize the various absorption times: (1,3] steps \square , (3,6] steps $\begin{smallmatrix} \square & \square & \square \\ \square & \square & \square \end{smallmatrix}$, (6,9] steps $\begin{smallmatrix} \square & \square & \square & \square \\ \square & \square & \square & \square \end{smallmatrix}$.

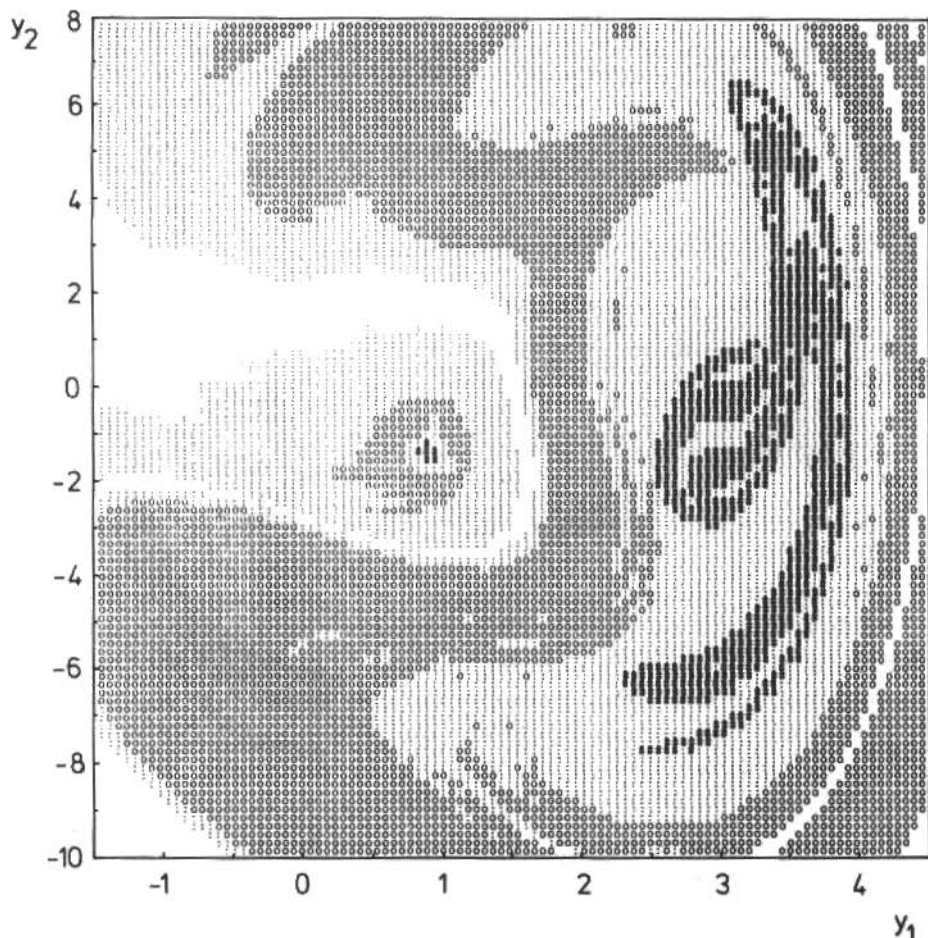


Figure 5. Expected absorption times of transient cells into persistent groups

For a complete understanding of the properties of dissipative nonlinear dynamical systems one has to use a variety of methods as described in this paper. If one would like to know more about the statistic behavior of the attractor one may look also at the limiting probability distribution. For a more detailed discussion of statistical properties of attractors, see Hsu, Kim [18] and [19].

CONCLUSION

The large number of possible motions of which a dissipative nonlinear system is capable has been studied in terms of attractors. A classification can be made based on fundamental properties of attractors. The global behavior of nonlinear dynamical systems can be analyzed by using the cell mapping theory. The probabilistic formulation led to a description of the dynamics by means of a Markov chain. By assuming that the probability distribution of the initial states is known, we can determine, as time increases, how the trajectories are distributed in the phase space. In this way the attractors of the dynamical systems are found and analyzed. Because of growing interest in nonlinear problems in mechanical systems the cell mapping theory may become more widely used as a tool for analysis.

REFERENCES

- [1] Ruelle, D. - Small random perturbations of dynamical systems and the definition of attractors. Commun. Math. Phys., 82 : 137-151 (1981).
- [2] Eckmann, J.-P. - Roads to turbulence in dissipative dynamical systems. Reviews of Modern Phys., 53 : 643-654 (1981).
- [3] Farmer, J.D. - Order within chaos. Univ. of California, Santa Cruse, Doctoral Diss., 1981.
- [4] Guckenheimer, J. - Noise in chaotic systems. Nature, 298 : 358-361 (1982).
- [5] Smale, S. - Differentiable dynamical systems. Bull. Amer. Math. Soc., 73 : 747-817 (1967).
- [6] Kaplan, J. and Yorke, J. - Chaotic behavior of multidimensional difference equations. In: Functional Differential Equations and Approximation of Fixed Points, H.-O. Peitgen, H.O. Walther (eds.), Berlin/...: Springer-Verlag (1979) 228-237.

- [7] Hsu, C.S. - A theory of cell-to-cell mapping dynamical systems. J. of Appl. Mech., 47 : 931-939 (1980).
- [8] Hsu, C.S. - A generalized theory of cell-to-cell mapping for nonlinear dynamical systems. J. of Appl. Mech., 48 : 634-642 (1981).
- [9] Hsu, C.S. and Guttalu, R.S. - An unravelling algorithm for global analysis of dynamical systems: an application of cell-to-cell mappings. J. of Appl. Mech., 47 : 940-948 (1980).
- [10] Hsu, C.S.; Guttalu, R.S. and Zhu, W.H. - A method of analyzing generalized cell mappings. J. of Appl. Mech., 49 : 885-994 (1982).
- [11] Bestle, D. and Kreuzer, E. - A modification and extension of an algorithm for generalized cell mapping. To appear in Computer Methods in Applied Mechanics and Engineering.
- [12] Kreuzer, E. - Zur numerischen untersuchung nichtlinearer dynamischer systeme. Stuttgart, Universität, Habil.-Schr. (1986).
- [13] Farmer, J.D. - Information dimension and the probabilistic structure of chaos. Z. Naturforschung 37a (1982) 1304-1325.
- [14] Lichtenberg, A.J. and Lieberman, M.A. - Regular and stochastic motion, Berlin/...: Springer-Verl. 1983.
- [15] Pesin, Ya.B. - Characteristic Lyapunov exponents and smooth ergodic theory. Russian Math. Surveys, 32 : 55-114 (1977).
- [16] Ueda, Y. - Steady motions exhibited by Duffing's equation: a picture book of regular and chaotic motions. In: New approaches to nonlinear problems in dynamics, P.J. Holmes (ed.), Philadelphia: SIAM 1980.
- [17] Kleczka, M. - Zur berechnung der Lyapunov-Exponenten und deren Bedeutung. Stuttgart, Universität, Inst. B für Mech., Student Thesis STUD-16.
- [18] Hsu, C.S. and Kim, M.C. - Statistics of strange attractors by generalized cell mapping. J. of Stat. Phys., 38 : 735-761 (1985).
- [19] Kreuzer, E.J. - Analysis of chaotic systems using the cell mapping approach. Ing. Arch., 55 : 285-294 (1985).

NOTICIÁRIO

II ENCONTRO DE EDITORES DE REVISTAS CIENTÍFICAS

PROMOÇÃO: CNPQ E FINEP
SÃO PAULO, SP, 27 E 28 DE NOVEMBRO DE 1985

DOCUMENTO FINAL

A. Premissas

1. A política de divulgação científica e tecnológica é parte integrante da política global de ciência e tecnologia do país e, por consequência, o financiamento desta atividade deverá constar nos orçamentos e nos programas de Pesquisa e Desenvolvimento das agências financiadoras e outras instituições.

Para adequar os recursos às reais necessidades do setor, seriam necessários, no mínimo, 2% dos recursos efetivamente alocados à Pesquisa e Desenvolvimento pelas agências financiadoras e pelas instituições de pesquisa.

2. O pesquisador brasileiro deve ser conscientizado de sua responsabilidade na publicação ampla dos resultados de seu trabalho em revistas científicas nacionais.
3. Os progressos da pesquisa científica e tecnológica do país, estão exigindo um salto qualitativo e quantitativo na informação científica e tecnológica.
4. Deve ser reconhecida a importância das revistas científicas como espelho da produção científica nacional.

B. Recomendações às Agências Financiadoras e Órgãos Públicos

1. Que as agências financiadoras estudem mecanismos de pagamento de salários às equipes de editoração científica, visando criar estruturas profissionais;
2. que o Ministério da Educação destine recursos às bibliotecas universitárias para assinatura de revistas científicas nacionais de boa qualidade;

3. que as agências coordenadoras do Programa Setorial de Publicações em Ciência e Tecnologia concedam - por tempo determinado - um adicional de 15% sobre o total de recursos fornecidos a cada revista, para que a entidade responsável pela publicação em via 200 exemplares a bibliotecas, entidades e grupos de sua área de especialização localizados no Brasil e 100 exemplares para bibliotecas congêneres no exterior. Tais recursos adicionais destinam-se a cobrir os custos com manipulação, embalagem e postagem dos exemplares. Os editores proporão as entidades a serem contempladas, para referendo pela agência financiadora;
4. que haja maior pontualidade na liberação dos recursos pelos órgãos financiadores. A notificação da aprovação e valor do financiamento deve ser imediata, para fins de planejamento;
5. que a avaliação de revistas científicas da mesma área por parte das agências financiadoras seja feito em conjunto para melhor julgamento;
6. que as agências financiadoras criem mecanismos de estímulo à publicação, em revistas científicas nacionais, dos resultados dos projetos de pesquisa por elas financiados. Tal estímulo deve ser estendido à publicação de resumos e/ou artigos baseados em teses de pós-graduação;
7. que a Finep estimule as pequenas e médias empresas nacionais, por ela financiadas, a veicular anúncios de seus produtos nas revistas científicas nacionais, e
8. que haja uma maior articulação entre as agências financiadoras.

C. Recomendações aos Editores

1. Que as revistas científicas procurem ter uma abrangência nacional;
2. que sejam obedecidos certos padrões editoriais mínimos e normas técnicas, tais como: títulos, legendas, resumos, palavras-chave em português e inglês, bibliografias com dados completos etc;
3. que a Associação Brasileira de Editores Científicos (ABEC) difunda as revistas científicas nacionais em eventos como feitas de livros, congressos e reuniões;

4. que haja intercâmbio de anúncios padronizados entre as revistas nacionais, bem como as congêneres do exterior. A ABEC deve estudar a criação de um **pool** de publicidade;
5. que os **referees** recebam os pareceres de outros **referees** quando da apreciação de um mesmo trabalho;
6. que haja uma maior promoção das revistas nacionais nos países do terceiro mundo, particularmente nos de língua portuguesa e espanhola;
7. que se organize a administração das revistas e racionalize o trabalho de editoração, com a progressiva profissionalização das equipes, e
8. que as revistas publiquem o documento final do II Encontro de Editores de Revistas Científicas.

D. Recomendações às Agências e aos Editores

1. Estimular a existência de pelo menos uma revista científica de bom nível em cada área do conhecimento;
2. maior agressividade e profissionalização na difusão das revistas;
3. no processo de avaliação de pesquisadores, técnicos e professores devem ser considerados em pé de igualdade suas contribuições em revistas nacionais de bom nível e em revistas internacionais;
4. a regularidade das publicações é uma meta a ser atingida pelas revistas para aumentar sua credibilidade e possibilitar sua indexação nos órgãos nacionais e estrangeiros;
5. para melhor adequação do percentual financiado pelas agências, os orçamentos devem passar a incluir todos os custos, entre os quais a remuneração dos editores e equipes;
6. os alunos de graduação e de pós-graduação devem ser considerados como um público a ser também atingido pela comunicação científica e tecnológica;
7. o II Encontro recomenda que seja constituída no prazo de 60 dias uma comissão composta de representantes das agências financia-

doras e da ABEC com o objetivo de elaborar um documento sobre política de publicação técnico-científica no Brasil, a ser amplamente divulgado, e

8. os participantes do II Encontro apoiam o projeto de mensuração de revista Ciência Hoje.

